Atmos. Chem. Phys. Discuss., 14, 32427–32489, 2014
www.atmos-chem-phys-discuss.net/14/32427/2014/
doi:10.5194/acpd-14-32427-2014
© Author(s) 2014. CC Attribution 3.0 License.

Atmospheric Chemistry and Physics Discussions

This discussion paper is/has been under review for the journal Atmospheric Chemistry and Physics (ACP). Please refer to the corresponding final paper in ACP if available.

Investigating the links between ozone and organic aerosol chemistry in a biomass burning plume from a prescribed fire in California chaparral

M. J. Alvarado[1], C. R. Lonsdale[1], R. J. Yokelson[2], S. K. Akagi[2], H. Coe[3], J. S. Craven[4], E. V. Fischer[5], G. R. McMeeking[5], J. H. Seinfeld[4], T. Soni[1,*], J. W. Taylor[3], D. R. Weise[6], and C. E. Wold[7]

[1]Atmospheric and Environmental Research, Lexington, MA, USA
[2]Department of Chemistry, University of Montana, Missoula, MT, USA
[3]Centre for Atmospheric Science, University of Manchester, Manchester, UK
[4]Division of Chemistry and Chemical Engineering, California Institute of Technology, Pasadena, CA, USA
[5]Colorado State University, Department of Atmospheric Science, Fort Collins, CO, USA
[6]PSW Research Station, USDA Forest Service, Riverside, CA, USA
[7]Fire Sciences Laboratory, United States Department of Agriculture (USDA) Forest Service, Missoula, MT, USA
[*]now at: Shell Chemical LP, Houston, Texas, USA

Received: 8 November 2014 – Accepted: 24 November 2014 – Published: 21 December 2014

Correspondence to: M. J. Alvarado (malvarad@aer.com)

Published by Copernicus Publications on behalf of the European Geosciences Union.

ACPD
14, 32427–32489, 2014

Abstract

Within minutes after emission, rapid, complex photochemistry within a biomass burning smoke plume can cause large changes in the concentrations of ozone (O_3) and organic aerosol (OA). Being able to understand and simulate this rapid chemical evolution under a wide variety of conditions is a critical part of forecasting the impact of these fires on air quality, atmospheric composition, and climate. Here we use version 2.1 of the Aerosol Simulation Program (ASP) to simulate the evolution of O_3 and secondary organic aerosol (SOA) within a young biomass burning smoke plume from the Williams prescribed burn in chaparral, which was sampled over California in November 2009. We demonstrate the use of a method for simultaneously accounting for the impact of the unidentified semi-volatile to extremely low volatility organic compounds (here collectively called "SVOCs") on the formation of OA (using the Volatility Basis Set) and O_3 (using the concept of mechanistic reactivity). We show that this method can successfully simulate the observations of O_3, OA, PAN, NO_x, and C_2H_4 to within measurement uncertainty using reasonable assumptions about the chemistry of the unidentified SVOCs. These assumptions were: (1) a reaction rate constant with OH of $\sim 10^{-11}$ cm^3 s^{-1}, (2) a significant fraction (~ 50 %) of the $RO_2 + NO$ reaction resulted in fragmentation, rather than functionalization, of the parent SVOC, (3) ~ 1.1 molecules of O_3 were formed for every molecule of SVOC that reacted, (4) ~ 60 % of the OH that reacted with the unidentified SVOCs was regenerated as HO_2, and (5) that ~ 50 % of the NO that reacted with the SVOC peroxy radicals was lost, presumably to organic nitrate formation. Additional evidence for the fragmentation pathway is provided by the observed rate of formation of acetic acid, which is consistent with our assumed fragmentation rate. This method could provide a way for classifying different smoke plume observations in terms of the average chemistry of their SVOCs, and could be used to study how the chemistry of these compounds (and the O_3 and OA they form) varies between plumes.

ACPD
14, 32427–32489, 2014

1 Introduction

Biomass burning is a major source of atmospheric trace gases and particles that impact air quality and climate (e.g., Crutzen and Andreae, 1990; van der Werf, 2010; Akagi et al., 2011). Within minutes after emission, rapid and complex photochemistry within the young biomass burning smoke plumes can lead to significant increases in the concentrations of secondary pollutants such as ozone (O_3, e.g. Mauzerall et al., 1998; Goode et al., 2000; Hobbs et al., 2003; Pfister et al., 2006; Lapina et al., 2006; Val Martin et al., 2006; Yokelson et al., 2009; Jaffe and Widger, 2012; Akagi et al., 2012, 2013), peroxyacetyl nitrate (PAN, e.g. Jacob et al., 1992; Alvarado et al., 2010, 2011; Fischer et al., 2014), and organic aerosol (OA, e.g. Hobbs et al., 2003; Grieshop et al., 2009a, b; Yokelson et al., 2009; Hennigan et al., 2011; Heringa et al., 2011; Vakkari et al., 2014) after less than an hour of aging, while other smoke plumes can show little to no formation of O_3 (e.g. Alvarado et al., 2010; Zhang et al., 2014) or OA (e.g. Akagi et al., 2012). Understanding the atmospheric chemistry of these young smoke plumes, especially which conditions can lead to the secondary formation of O_3, PAN, and OA, is thus critical to understanding the impact of these plumes on atmospheric composition and the resulting impacts on air quality, human health, and climate. However, global- and regional-scale Eulerian models of atmospheric chemistry artificially dilute biomass burning emissions into large-scale grid boxes, which can result in large errors in the predicted concentrations of O_3 and aerosol species downwind (e.g., Alvarado et al., 2009; Zhang et al., 2014). In contrast, plume-scale Lagrangian models allow us to examine the chemical and physical transformations within these concentrated plumes in detail and can be used to develop parameterizations for this aging process for coarser models (e.g., the parameterizations of Vinken et al., 2011 and Holmes et al., 2014 for ship plumes).

Our understanding of the formation of ozone within biomass burning plumes is still poor, due both to the limited observational data available on O_3 formation in smoke plumes and the highly variable results seen in the available observations. Several air-

ACPD
14, 32427–32489, 2014

craft and surface studies of the chemistry of young biomass burning smoke plumes have found significant formation of O_3 within smoke plumes. For example, Baylon et al. (2014) reported $\Delta O_3/\Delta CO$ from 0.4 to 11 %, corresponding to O_3 enhancements of 3.8 to 32 ppbv in 19 wildfire plumes samples at Mt. Bachelor Observatory. They note that plumes that have low values of $\Delta O_3/\Delta CO$ can still correspond to significant O_3 enhancements in concentrated plumes, with one event with a $\Delta O_3/\Delta CO$ value of 0.81 % corresponding to an O_3 enhancement of 17 ppbv. Akagi et al. (2013) found significant O_3 formation ($\Delta O_3/\Delta CO$ from 10–90 %) within two hours for all of the South Carolina prescribed fires studied, and Parrington et al. (2013) found values of $\Delta O_3/\Delta CO$ increased from 2.0 ± 0.8 % in boreal biomass burning plumes less than 2 days old over Eastern Canada to 55 ± 29 % in plumes that were more than 5 days old. Similarly, Andreae et al. (1994) found that aged plumes (over 10 days old) from the biomass burning regions of South America and Africa had $\Delta O_3/\Delta CO$ values between 20–70 %. However, other studies, mainly in boreal regions, have found little formation or even depletion of O_3 in some young biomass burning plumes (e.g., Alvarado et al., 2010). This low O_3 formation is likely due to a combination of low emissions of NO_x from the boreal fires (Akagi et al., 2011), sequestration of NO_x in PAN and other organic nitrates (e.g., Jacob et al., 1992; Alvarado et al., 2010, 2011), and reduced rates of photochemical reactions due to aerosol absorption and scattering (e.g. Jiang et al., 2012). Similarly, some studies have shown that fires can contribute to high surface O_3 events that exceed the US air quality standard for O_3 (e.g., Jaffe et al., 2013), but other studies suggest that this enhanced surface O_3 is only present when the biomass burning emissions mix with anthropogenic pollution (Singh et al., 2012; Zhang et al., 2014). However, even given the observed variability among fires, it is likely that biomass burning has an impact on the concentrations of tropospheric O_3. For example, the recent review of Jaffe and Widger (2012) estimated that biomass burning could contribute 170 Tg of O_3 per year, accounting for 3.5 % of all global tropospheric O_3 production. However, Sudo and Akimoto (2007) estimated that over a third of tropospheric O_3 came

ACPD
14, 32427–32489, 2014

from free troposphere chemical production due to biomass burning outflow from South America and South Africa.

The NO_x emitted by biomass burning is rapidly converted into a wide variety of inorganic nitrate (i.e. $HNO_{3(g)}$ and total aerosol inorganic nitrate, or $NO_{3(p)}$) and organic nitrate species (i.e. alkyl nitrates ($RONO_2$) and peroxy nitrates (RO_2NO_2), including PAN; Jacob et al., 1992; Yokelson et al., 2009; Alvarado et al., 2010, 2011; Akagi et al., 2012). The rate at which this conversion occurs and the relative production of inorganic nitrate, alkyl nitrates, and peroxy nitrates are a key control of the impact of the biomass burning on O_3 production and atmospheric composition. Once NO_x is converted to inorganic or organic nitrate, it is generally unavailable for further O_3 formation near the fire source. Furthermore, while conversion of NO_x into inorganic nitrate ($HNO_{3(g)} + NO_{3(p)}$) is generally irreversible (except for the slow reaction of $HNO_{3(g)}$ with OH), peroxy nitrate species like PAN can act as thermally unstable reservoirs of NO_x, allowing transport of NO_x in the upper atmosphere far from the original source and then producing NO_x via thermal decomposition as the airmass descends to the surface (e.g., Fischer et al., 2010). This regenerated NO_x can thus impact O_3 formation far from the original source.

In addition, photochemistry within the smoke plume can rapidly oxidize non-methane organic compounds (NMOCs), both those that were emitted in the gas phase and those emitted in the particle phase, lowering their vapor pressure and thus leading to the formation of secondary organic aerosol (SOA). As with O_3 and PAN formation, the formation of SOA in smoke plumes is highly variable, with the ratio of OA to CO_2 increasing by a factor of 2–3 downwind of some biomass burning fires (e.g. Hobbs et al., 2003; Grieshop et al., 2009a, b; Yokelson et al., 2009; Hennigan et al., 2011; Heringa et al., 2011; Vakkari et al., 2014), while in others it can stay constant or even decrease (e.g. Capes et al., 2008; Akagi et al., 2012). For cases where little net SOA formation was observed, it is likely that the NMOCs were still being oxidized. However, in these cases the fragmentation of the organic species after oxidation (leading to higher volatility products) is likely more common than functionalization (i.e. the addition of oxygen to the organic species, leading to lower volatility products).

ACPD
14, 32427–32489, 2014

Plume-scale Lagrangian parcel models can be used to investigate the evolution of O_3, PAN, and OA in smoke plumes in detail, as their relatively simple parameterizations of plume dispersion and transport allow detailed simulation of the chemical and microphysical processes taking place within the young smoke plumes (e.g., Mauzerall et al., 1998; Mason et al., 2001, 2006; Jost et al., 2003; Trentmann et al., 2005; Alvarado and Prinn, 2009; Arnold et al., 2014; Heilman et al., 2014). Previous plume-scale modeling studies have greatly advanced our understanding of these transformations. Mauzerall et al. (1998) found that O_3 production within biomass burning plumes was limited by the concentration of NO_x and that the formation and subsequent degradation of peroxy acetyl nitrate (PAN) helped to maintain NO_x concentrations. Mason et al. (2001) and Trentmann et al. (2003) showed that oxygenated volatile organic compounds (OVOCs) were critical to the formation of O_3 within the smoke plumes. More recent work has suggested heterogeneous chemistry and currently unidentified organic species as potential explanations for the rapid formation of O_3 and organic aerosol seen within some smoke plumes (Trentmann et al., 2005; Mason et al., 2006; Alvarado and Prinn, 2009).

The Aerosol Simulation Program (ASP) was developed to simulate the formation of ozone and secondary organic aerosol (SOA) within young biomass burning plumes (Alvarado, 2008). ASP v1.0 was used to simulate several African and North American plumes (Alvarado and Prinn, 2009) and to simultaneously simulate the chemistry, dynamics, and radiative transfer within a smoke plume using a high-resolution three-dimensional plume model (Alvarado et al., 2009). Alvarado and Prinn (2009) showed while their initial ASP v1.0 simulations underestimated the formation of both OH and O_3 in the Timbavati savannah fire smoke plume (Hobbs et al., 2003), if the OH concentration in ASP v1.0 was fixed at the estimated value of 1.7×10^7 molecules cm^{-3} then the model was able to reproduce the observed concentrations of O_3. This suggested that the model was missing an important source of OH, and they proposed a heterogeneous reaction of NO_2 on aerosol particles producing HONO, followed by the photolysis of HONO into NO and OH, as a candidate for the missing source of OH within the smoke plume. Alvarado and Prinn (2009) also found that including only

ACPD
14, 32427–32489, 2014

SOA formation from known SOA precursors (mainly aromatic species like toluene) underestimated the concentrations of organic aerosol observed downwind by ~60 %, suggesting that the model was missing a large source of SOA. They proposed that the large amount of gas-phase organic compounds that were unidentified by the then current measurement techniques (Christian et al., 2003; Warneke et al., 2011) could include the precursors for the missing SOA. Assuming these compounds had SOA yields similar to monoterpenes gave the observed SOA formation.

In this paper, we describe recent updates to the gas-phase chemistry and secondary organic aerosol (SOA) formation modules in ASP. We use this updated version (ASP v2.1) to simulate the chemical evolution of a young biomass burning smoke plume sampled over California in November near San Luis Obispo (the Williams Fire, Akagi et al., 2012). The analysis of the O_3, PAN, and OA evolution in biomass burning plumes is complicated by the fact that a large fraction (30–50 % by carbon mass, Christian et al., 2003; Warneke et al., 2011) of the NMOCs present in smoke plumes are unidentified, and thus their oxidation chemistry is not well known. We present a method for simultaneously accounting for the impact of the unidentified organic compounds (here collectively called "SVOCs") on the formation of OA and O_3. We show that this method can successfully simulate the Williams Fire plume observations using reasonable assumptions about the chemistry of the unidentified SVOCs.

Section 2 describes the updates to the gas-phase chemistry and secondary organic aerosol formation modules of ASP for version 2.1. Section 3 discusses our validation of the gas-phase chemistry in ASP v2.1 against data from a smog chamber (Carter et al., 2005). Section 4 describes the Williams Fire and summarizes the available observations of the smoke plume from Akagi et al. (2012). Section 5 discusses the results of the ASP simulation of the Williams Fire, including sensitivity tests to investigate the chemistry of the unidentified SVOCs and their impacts on O_3, PAN, other trace gases, and OA, while Sect. 6 gives the conclusions of our study and directions for future work.

ACPD
14, 32427–32489, 2014

2 Updates to the Aerosol Simulation Program (ASP)

An overview of ASP v1.0 is given by Alvarado and Prinn (2009), and the routines are described in detail in Alvarado et al. (2008). Here we briefly discuss the modules of ASP that have not changed since Alvarado and Prinn (2009) in Sect. 2.1 before describing the updates to the gas-phase chemistry (Sect. 2.2) and SOA formation (Sect. 2.3) routines for ASP v2.1.

2.1 ASP modules

Aerosols are represented in ASP by a single moving-center sectional size distribution (Jacobson, 1997, 2002, 2005). ASP includes modules to calculate aerosol thermodynamics, gas-to-aerosol mass transfer (condensation/evaporation), and coagulation of aerosols. The thermodynamics module in ASP uses the Mass Flux Iteration (MFI) method of Jacobson (2005) to calculate the equilibrium concentration of gas and aerosol species. Equilibrium constants for the inorganic electrolyte reactions match those of Fountoukis and Nenes (2007). Binary activity coefficients of inorganic electrolytes are calculated using the Kusik–Meissner method (Kusik and Meissner, 1978; Resch, 1995), as are the mean activity coefficients. The water content of inorganic aerosols is calculated with an iterative routine that calculates water activities for aqueous solutions of a single electrolyte using a formula based on the Gibbs–Duhem equation (Steele, 2004). Steele (2004) and Alvarado (2008) found this approach compares well with other inorganic aerosol thermodynamics models such as ISORROPIA (Nenes et al., 1998; Fountoukis and Nenes, 2007).

Mass transfer between the gas and aerosol phases is calculated in ASP using a hybrid scheme where the flux-limited kinetic equations governing the condensation/evaporation of H_2SO_4 and organic species are integrated, whereas NH_3, HNO_3, and HCl are assumed to be in equilibrium (Alvarado, 2008). Aerosol coagulation is calculated using the semi-implicit scheme of Jacobson (2005) with a Brownian coagulation kernel.

ACPD
14, 32427–32489, 2014

2.2 Gas-phase chemistry updates

The gas-phase chemistry within the ASP model for Version 2.1 has been completely revised from ASP v1.0, which used the CalTech Atmospheric Chemistry Mechanism (CACM, Griffin et al., 2005). The revised ASP v2.1 gas phase chemical mechanism includes 1608 reactions between 621 species. Examples of the gas-phase species input file and the reaction mechanism input file for ASP v2.1, along with other key chemical input files, are included in the Supplement.

All inorganic gas-phase chemistry within ASP v2.1 was updated to follow the IUPAC recommendations (Atkinson et al., 2004; updated data downloaded from http://iupac.pole-ether.fr/, accessed June 2012). We also tested the JPL recommendations (Evaluation #17, Sander et al., 2011) for these rate constants, but found that the differences between the recommendations generally made little difference to the model simulations, and as the IUPAC values were closer to those in ASP v1.0, these values were used.

All gas-phase chemistry for organic compounds containing 4 carbons or less has been "unlumped," i.e. the chemistry for each individual organic compound is explicitly resolved. This was done by following the reactions of the Leeds Master Chemical Mechanism (MCM) v3.2 (http://mcm.leeds.ac.uk/MCM/, accessed June 2012; Jenkin et al., 1997, 2003; Saunders et al., 2003; Bloss et al., 2005) for these species.

The chemical mechanism of isoprene within ASP v2.1 has been updated to follow the Paulot et al. (2009a, b) isoprene scheme, as implemented in GEOS-Chem and including corrections based on more recent studies (e.g., Crounse et al., 2011, 2012). The (lumped) chemistry for all other organic compounds in ASP has been updated to follow the Regional Atmospheric Chemistry Mechanism (RACM) v2 (Goliff et al., 2013). We chose RACM2 over the SAPRC-07 (Carter, 2010) and CB05 (Yarwood et al., 2005) lumped chemical mechanisms as the treatment of peroxy radicals in the RACM2 mechanism was more similar to the treatment in the Leeds MCM and the Paulot isoprene scheme, resulting in a more consistent chemical mechanism for ASP v2.1.

ACPD
14, 32427–32489, 2014

Photolysis rates are calculated offline using the Tropospheric Ultraviolet and Visible (TUV) radiation model version 5.0 (Madronich and Flocke, 1998) for 15 min increments, which are then linearly interpolated in ASP. Alvarado and Prinn (2009) assumed a "clear sky" radiation field that ignored the effect of aerosol absorption and scattering on the calculated photolysis rates. Here we instead estimate the time-dependent aerosol, O_3, SO_2, and NO_2 concentrations within the smoke plumes and calculate their effect on the photolysis rates at different heights within the plume (see Sect. 5.1 for details on how this was done for the Williams Fire).

2.3 SOA formation updates

We have updated the SOA formation module to follow the semi-empirical Volatility Basis Set (VBS) model of Robinson et al. (2007). Our implementation of this scheme followed the approach used by Ahmadov et al. (2012) to link the VBS scheme with the RACM chemical mechanism within WRF-Chem. We use 9 surrogates or "bins" for semi-volatile, intermediate volatility, low volatility, and extremely low volatility organic compounds (hereafter collectively referred to as "SVOCs" for simplicity) as in Dzepina et al., 2009, rather than only 4 as in Ahmadov et al. (2012). The saturation mass concentration at 300 K (C^*, see Robinson et al., 2007) of each SVOC differs by a factor of 10, and covers the range from 0.01 to 1.0×10^6 $\mu g\,m^3$. Following the Model to Predict the Multiphase Partitioning of Organics (MPMPO) of Griffin et al. (2003, 2005) and Pun et al. (2002), we assumed that an aqueous phase and a mixed hydrophobic organic phase are always present in the aerosol. Partitioning of organics between the gas and hydrophobic phase is governed by Raoult's law (assuming that all hydrophobic-phase OM is quasi-liquid and can dissolve organics as in Pankow, 1994a, b), while partitioning of organics into the aqueous phase is governed by Henry's law. Following Pun et al. (2002), we assumed that (1) there is no interaction between the aqueous phase inorganic ions and the aqueous phase organics, and thus no organic salt formation, and (2) the activity coefficients of the organic ions (formed by the dissociation of organic acids) are equivalent to those of the corresponding molecular solute. We further

ACPD
14, 32427–32489, 2014

assumed that the pH of the aqueous phase is dominated by the strong inorganic acids and bases, and that the pH effects of the dissociating organic acids are negligible.

Like most organic compounds, SVOCs will react with OH. Most mechanisms for this chemistry (e.g., Robinson et al., 2007; Dzepina et al., 2009; Grieshop et al., 2009a, b; Ahmadov et al., 2012) parameterize this chemistry by assuming that the SVOCs react with OH to form a lower volatility SVOC, as in the reaction:

$$\mathrm{SVOC}_i + \mathrm{OH} \xrightarrow{k_{\mathrm{OH}}} \mu\mathrm{SVOC}_{i-n} \quad \text{(R1)}$$

where μ is the relative mass gain due to oxidation (e.g. via O addition), k_{OH} is the reaction rate with OH, and n is the "volatility shift", or by how many factors of 10 to lower the C^* of the product with each OH reaction. This simplified chemistry can be extended to account for the fact that the SVOCs could fragment during oxidation, leading to higher volatility products:

$$\mathrm{SVOC}_i + \mathrm{OH} \xrightarrow{k_{\mathrm{OH}}} \mu(1-\alpha)\mathrm{SVOC}_{i-n} + \mu\alpha\mathrm{SVOC}_{i+1} + \alpha\mathrm{VOC}_j \quad \text{(R2)}$$

where α is the fraction of SVOC_i that fragments into SVOC_{i+1} and VOC_j. However, the highly simplified chemistry of Reactions (R1) or (R2) is not appropriate for situations where reactions with the SVOC compounds are a potentially significant sink of OH, such as in a concentrated smoke plume. Thus in ASP v2.1, the chemistry of the SVOCs is instead parameterized in a more realistic manner for a generic organic species, following the idea of "mechanistic reactivity" (e.g., Carter, 1994; Bowman and Seinfeld, 1994a, b; Seinfeld and Pandis, 1998). After reaction with OH SVOCs produce peroxy radicals (RO_2), which can react with NO to form NO_2 and HO_2, thereby regenerating OH and forming O_3. Reactions (R3) and (R4) show this more general chemical mechanism for the SVOCs:

$$\mathrm{SVOC}_i + \mathrm{OH} \xrightarrow{k_{\mathrm{OH}}} \mathrm{RO}_{2,i} \quad \text{(R3)}$$

$$\mathrm{RO}_{2,i} + \chi\mathrm{NO} \xrightarrow{k_{\mathrm{RO}_{2,i}}} \mu(1-\alpha)\mathrm{SVOC}_{i-n} + \mu\alpha\mathrm{SVOC}_{i+1} + \alpha\mathrm{VOC}_j + \beta\mathrm{NO}_2 + \delta\mathrm{HO}_2 \quad \text{(R4)}$$

ACPD
14, 32427–32489, 2014

where $k_{RO_{2,i}}$ is assumed to be 4.0×10^{-12} cm^3 molecule^{-1} s^{-1} based on the reaction rate for the peroxy radicals from long-chain alkanes and alkenes with NO in RACM2 (Goliff et al., 2013). We can see that $\chi - \beta$ is the number of NO_x lost (implicitly via the addition of a nitrate group to the product SVOCs), $1 - \delta$ is the number of HO_x lost, and $\beta + \delta$ is the number of O_3 made per reaction (by subsequent reactions of NO_2 and HO_2 to generate O_3). For example, the values for long-chain alkanes (HC8) in the $RACM_2$ mechanism (Goliff et al., 2013) would be $\chi = 1$, $\delta = 0.63$, and $\beta = 0.74$, such that 0.26 NO_x and 0.37 HO_x are lost and 1.37 O_3 are formed per reaction. Note that the mechanism of Reactions (R3) and (R4) is still highly simplified: we assume that reaction of SVOC with OH always produces a RO_2 radical, and that the RO_2 produced does not react with HO_2 or another RO_2. Our purpose is less to detail all the possible reactions of the unidentified SVOCs and more to explore how their average chemistry might affect O_3 and OA evolution in smoke plumes.

We also adjusted the calculation of aerosol water content to use the "kappa" (κ) parameterization of organic hygroscopicity (Petters and Kreidenweis, 2007) for the lumped SVOCs. In this parameterization, the hygroscopicity parameter κ for the organic species is defined as:

$$\frac{1}{a_w} = 1 + \kappa \frac{V_{s,i}}{V_{w,i}} \quad (1)$$

where a_w is the activity of water in the solution (equal to the relative humidity at equilibrium), $V_{s,i}$ is the volume of the dry organic solute i and $V_{w,i}$ is the volume of water in the solution. The water content calculated for each organic species, along with that calculated for the inorganic solution ($V_{w,inorg}$ see Sect. 2.1 above) are then combined using the Zdanovskii, Stokes, and Robinson (ZSR) approximation (Zdanovskii, 1948; Stokes and Robinson, 1966):

$$V_w = \frac{a_w}{1 - a_w} \sum_i \kappa_i V_{s,i} + V_{w,inorg} \quad (2)$$

ACPD
14, 32427–32489, 2014

3 ASP photochemistry evaluated with smog chamber data

To evaluate the performance of the updated photochemical mechanism in ASP v2.1 in predicting the formation of ozone, several test simulations were performed to compare the results of the mechanism to laboratory smog chamber data. This comparison provides us with a baseline for interpreting the results of our simulation of O_3 formation in the Williams Fire in Sect. 5. The data used for the comparison came from the EPA chamber of Carter et al. (2005). This chamber consists of two collapsible 90 m^3 FEP Teflon reactors (chambers A and B) mounted on pressure-controlled moveable frameworks inside a temperature-controlled room flushed with purified air. Solar radiation is simulated in the chamber using a 200 kW Argon arc lamp for all experiments considered here.

Table 1 shows the temperature and initial reactant concentrations used in our model to simulate each chamber study. All model simulations were performed at a pressure of 1000 mbar, a relative humidity of 1 %, and a CH_4 concentration of 1800 ppbv. The temperature and concentration data were provided by William P. L. Carter (http://www.cert.ucr.edu/$~$carter/SAPRC/SAPRCfiles.htm, accessed March 2014). The EPA chamber runs used an 8 compound surrogate for ambient VOC concentrations, consisting of formaldehyde, ethylene, propene, trans-2-butene, n-butane, n-octane, toluene, and m-xylene (Carter et al., 1995, 2005). The initial concentrations of HONO were extrapolated from CO-NO_x and n-butane-NO_x runs to account for the potential chamber radical source (Carter et al., 2005).

Table 2 presents the rates of off-gassing, wall reaction rates, and selected photolysis rates for the chamber experiments considered here. The off-gassing rate for HONO was determined as the rate that enabled the SAPRC-99 chemical mechanism (Carter, 2000) to best predict the O_3 formation observed in CO-air, HCHO-air and CO-HCHO-air experiments performed within the chamber (Carter et al., 2005). The rate in Chamber A was found to be slightly higher than that in Chamber B, so different values are used for the chambers. The off-gassing rate of HCHO was chosen to match the low but

ACPD
14, 32427–32489, 2014

measurable amount of formaldehyde found even in pure air and CO-NO_x experiments in the chamber. Heterogeneous wall loss reaction rates for O_3, NO_2, and N_2O_5 were also estimated from reactor observations (Carter et al., 2005). The photolysis rate of NO_2 in the chambers was measured directly, and scaling factors for the other photolysis rates were calculated by Carter et al. (2005) from the relative spectral intensity of the arc lamp.

Following Carter et al. (2005), we evaluated the ability of our mechanism to simulate the total amount of NO oxidized and O_3 formed in the experiments, measured as $\Delta([O_3] - [NO])_t \equiv ([O_3]_t - [NO]_t) - ([O_3]_{initial} - [NO]_{initial})$. The hourly results of the comparisons for $\Delta([O_3] - [NO])$ are presented in Fig. 1a. We can see that the ASP v2.1 mechanism tends to underestimate $\Delta([O_3] - [NO])$, with a mean absolute bias of −24.6 ppbv and a mean normalized bias of −22.4 %. Comparisons of the ASP calculations for O_3, NO, and NO_x (not shown) show that this model underestimate of $\Delta([O_3] - [NO])$ is primarily due to the model underestimating O_3 formation, rather than underestimating the loss of NO or NO_x. Similarly, the ASP v2.1 calculations for the concentrations of the organic gas species matches well with the chamber measurements (not shown) except for formaldehyde (HCHO) (see Fig. 1b), where the secondary formation of HCHO appears to be underestimated. Figure 2 shows the bias in $\Delta([O_3] - [NO])$ vs. the initial ratio of the mixing ratio of reactive organic gases (ROGs, e.g., the concentration of the surrogate gases in ppm C) to the mixing ratio of NO_x (in ppm N). We can see that the bias is between 0 and −10 % for ROG/NO_x ratios greater than 30, but increases to −40 to −50 % for "high NO_x" cases (ROG/NO_x ratios $\ll$ 20). For comparison, the initial ROG/NO_x ratio in biomass burning smoke can range from ∼ 10–100 (Akagi et al., 2011, assuming that the total NMOC mass is 1.6 times the mass of carbon in these compounds). Both the general underestimation of $\Delta([O_3] - [NO])$ and the increase of the negative bias at low ROG/NO_x concentrations is consistent with the behaviors of the SAPRC-99 (Carter et al., 2005), SAPRC-07 (Carter, 2010), and CB05 (Yarwood et al., 2005) mechanisms evaluated against the EPA chamber data. Carter (2010) noted that this under-prediction of O_3 at low ROG/NO_x ratios was ap-

ACPD
14, 32427–32489, 2014

parently linked to the presence of aromatics in the surrogate mixture, with comparisons of SAPRC-07 with EPA chamber runs with a non-surrogate mixture showing a positive bias of about +25 % for cases with low ROG/NO_x ratios.

4 Williams Fire data

The Williams Fire (34°41′45″ N, 120°12′23″ W) was sampled by the US Forest Service (USFS) Twin Otter aircraft from 10:50–15:20 LT on 17 November 2009 (Akagi et al., 2012). The fire burned approximately 81 ha of scrub oak woodland understory and coastal sage scrub. Skies were clear all day and RH was low (11–26 %) with variable winds (2–5 m s^{-1}). The Williams Fire smoke plume showed significant secondary production of O_3 and PAN, but the enhancement ratio of OA to CO_2 decreased slightly downwind (Akagi et al., 2012). In this study, we use the processed data from Akagi et al. (2012) that provided concentrations of several trace gases and OA measured during several quasi-Lagrangian transects of the Williams Fire. Full details on the measurements made and the processing of the data for the plume transects are given in Akagi et al. (2012); those used in this study are briefly described here.

4.1 Airborne Fourier Transform InfraRed spectrometer (AFTIR)

The University of Montana AFTIR system and the instruments described below were deployed on a US Forest Service (USFS) Twin Otter aircraft. The AFTIR was used to measure 21 gas-phase species: water vapor (H_2O), carbon dioxide (CO_2), carbon monoxide (CO), methane (CH_4), nitric oxide (NO), nitrogen dioxide (NO_2), ammonia (NH_3), hydrogen cyanide (HCN), nitrous acid (HONO), peroxy acetyl nitrate (PAN), ozone (O_3), glycolaldehyde ($HCOCH_2OH$), ethylene (C_2H_4), acetylene (C_2H_2), propylene (C_3H_6), formaldehyde (HCHO), methanol (CH_3OH), furan (C_4H_4O), phenol (C_6H_5OH), acetic acid (CH_3COOH), and formic acid (HCOOH). Ram air was directed through a halocarbon-wax coated inlet and into a Pyrex multipass cell. IR spectra were

ACPD
14, 32427–32489, 2014

collected at 1 Hz by directing the IR beam into the cell where it traversed a total path length of 78 m and was then focused onto an MCT detector. "Grab samples" of air were selected by closing the valves for 1–2 min to allow signal averaging. The IR spectra were analyzed to identify and quantify all detectable compounds. More details on the AFTIR system used are given by Yokelson et al. (1999, 2003).

4.2 Aerosol Mass Spectrometer (AMS)

An Aerodyne compact time-of-flight (CToF) aerosol mass spectrometer (herein referred to as AMS) measured aerosol chemical composition in a repeating cycle for 4 out of every 12 s during flight, including within the smoke plume. An isokinetic particle inlet sampling fine particles with a diameter cut-off of a few microns (Yokelson et al., 2007; Wilson et al., 2004) supplied the AMS. The AMS does not measure super-micron particles, so the inlet transmission should not have affected the results. In addition, particles smaller than 1 µm diameter account for nearly all the fine particle mass emitted by biomass fires (Radke et al., 1991; Reid et al., 2005b), so the composition analyses for fine particles should not have been affected by the lack of sensitivity to super-micron particles. The AMS collected sub-micron particles via an aerodynamic lens into a high vacuum particle sizing chamber. At the end of the particle sizing chamber, the particles impact a 600 °C vaporizer and filament assembly where they are vaporized and ionized by electron impact. The resulting molecular fragments are then extracted into an ion time-of-flight chamber where they are detected and interpreted as mass spectra. The AMS has been described in great detail elsewhere (Drewnick et al., 2005; Canagaratna et al., 2007). A collection efficiency of 0.5 (Huffman et al., 2005; Drewnick et al., 2003; Allan et al., 2004) was applied to the AMS data, which were processed to retrieve the mass concentration at standard temperature and pressure ($\mu g\,m^{-3}$, 273 K, 1 atm) for the major non-refractory particle species: OA, non-sea salt chloride, nitrate, sulfate, and ammonium, with < 36 % uncertainty.

ACPD
14, 32427–32489, 2014

4.3 Other measurements

Measurements of the ambient three-dimensional wind velocity, temperature, relative humidity, and barometric pressure at 1 Hz were obtained with a wing-mounted Aircraft Integrated Meteorological Measuring System probe (AIMMS-20, Aventech Research, Inc., Beswick et al., 2008). A 25 mm i.d. forward facing elbow "fast flow" inlet, collocated with the isokinetic and AFTIR inlets, fed air to a non-dispersive infrared instrument NDIR (LiCor model 7000) that measured CO_2 (at 0.5 Hz) from the third channel on the isokinetic particle inlet that also supplied the AMS, allowing the data from the AMS to be coupled to the trace gas data.

5 ASP simulation of Williams Fire

5.1 ASP setup

As in Alvarado and Prinn (2009), we simulated the Williams Fire smoke plume using ASP within a simple Lagrangian parcel model following Mason et al. (2001). We assume a Lagrangian parcel of fixed vertical extent (H, here assumed to be 1 km) and down-trajectory length (L), but variable cross-trajectory width $y(t)$. The temperature and pressure of the parcel are assumed to be constant. The full continuity equations for the Lagrangian parcel model are then

$$\frac{\mathrm{d}C_q}{\mathrm{d}t} = -\frac{4K_y}{\left(y_o^2 + 8K_y t\right)}\left(C_q - C_q^a\right) - \frac{v_\mathrm{d}}{H}C_q + \left(\frac{\mathrm{d}C_q}{\mathrm{d}t}\right)_{\mathrm{cond}} + \left(\frac{\mathrm{d}C_q}{\mathrm{d}t}\right)_{\mathrm{chem}} \quad (3)$$

$$\frac{\mathrm{d}n_i}{\mathrm{d}t} = -\frac{4K_y}{\left(y_o^2 + 8K_y t\right)}\left(n_i - n_i^a\right) - \frac{v_\mathrm{d}}{H}n_i + \left(\frac{\mathrm{d}n_i}{\mathrm{d}t}\right)_{\mathrm{cond}} + \left(\frac{\mathrm{d}n_i}{\mathrm{d}t}\right)_{\mathrm{coag}} \quad (4)$$

ACPD
14, 32427–32489, 2014

$$\frac{dc_{q,i}}{dt} = -\frac{4K_y}{\left(y_o^2 + 8K_y t\right)}\left(c_{q,i} - c^a_{q,i}\right) - \frac{v_d}{H}c_{q,i} + \left(\frac{dc_{q,i}}{dt}\right)_{cond} + \left(\frac{dc_{q,i}}{dt}\right)_{coag} + \left(\frac{dc_{q,i}}{dt}\right)_{chem} \quad (5)$$

where C_q is the concentration of gas-phase species (molecules cm^{-3} air), n_i is the number concentration of particles in size bin i (particles cm^{-3}), $c_{q,i}$ is the concentration of aerosol species q in size bin i (mol cm^{-3} air), y_o is the initial plume width (m), and K_y represents the horizontal diffusivity of the atmosphere (m^2 s^{-1}). The superscript a indicates the concentration of the given species in the atmosphere outside of the parcel (i.e., the background concentration).

The first term on the right-hand side of Eqs. (3)–(5) represents the effect of plume dispersion on the concentrations. Note that in y_o and K_y can be reduced to a single parameter, the initial dilution time scale $\tau_{mix,o}$:

$$-\frac{4K_y}{\left(y_o^2 + 8K_y t\right)} = -\frac{1}{\frac{y_o^2}{4K_y} + 2t} = -\frac{1}{\tau_{mix,o} + 2t} \quad (6)$$

The second term on the right hand side of Eqs. (3)–(5) is the effect of deposition on the concentrations, where v_d is the deposition velocity (m s^{-1}). We set the dry deposition velocity equal to 0 for gas-phase species, as the plume did not touch the ground during the modeled period, and use the size-dependent terminal velocity of the aerosol particles as the deposition velocity for aerosol species assuming a 1 km thick plume. As submicron aerosol dominated the aerosol mass in the smoke plume, this deposition of aerosol species has a negligible effect on the results, and given the low relative humidity during the Williams Fire, we also did not include wet deposition of particles or gases. The remaining terms represent the change in gas- and particle-phase concentrations

ACPD
14, 32427–32489, 2014

due to net mass transfer between the gas and aerosol phases (cond), coagulation of particles (coag), and chemical production and loss (chem).

The observed changes in CO mixing ratio were used to determine the best-fit model initial dilution time scale ($\tau_{\mathrm{mix},o}$ = 106.9 s) as well as upper and lower limits of the time scale ($\tau_{\mathrm{mix},o}(0)$ = 15.0 and 212.2 s, respectively), as shown in Fig. 3. The temperature of the plume was set at a constant value of 288.4 K, pressure of 880 hPa, and relative humidity of 15.7 % based on the observations of Akagi et al. (2012). The parcel was assumed to be emitted at 11:00 Pacific Standard Time (PST) and the model was integrated for 5 h. The integration of the different terms of the continuity Eqs. (3)–(5) were operator split for computational efficiency. The chemistry and mixing time steps were 1 s for the first 10 min of model integration due to the rapid dilution and chemical changes during this period, and were 60 s thereafter. The aerosol thermodynamics, condensation, and coagulation time steps were 60 s throughout.

The initial and background concentrations for the gas-phase inorganic and NMOC species are in Tables 3 and 4 gives the initial and background concentrations used for the aerosol species. Initial and background concentrations of trace gases and aerosols in the smoke were taken from observations of the Williams Fire (Akagi et al., 2012), where available. Emission ratios for other species were calculated using the literature reviews of Akagi et al. (2011) and Andreae and Merlet (2001). Other background concentrations were taken from runs of the GEOS-Chem model (Bey et al., 2001), run for our period as in Fischer et al. (2014). The volatility distribution for the POA was taken from the wood smoke study of Grieshop et al. (2009a, b). For all organic species, we assumed a constant κ = 0.04, corresponding to an O/C ratio of 0.25 (Jimenez et al., 2009) that is typical of biomass burning organic aerosol (Donahue et al., 2011). Since the relative humidity in the Williams Fire plume was very low, this assumption had little impact on our results. The initial smoke aerosol size distribution was assumed to be a log-normal with a geometric mean diameter D_{g} of 0.10 µm and a SD σ of 1.9 based on Reid and Hobbs (1998) for flaming combustion of Brazilian cerrado, which structurally is a similar mix of shrubs and grasses as in the Williams Fire. The initial

ACPD
14, 32427–32489, 2014

total number concentration of aerosol particles (2.34×10^6 particles cm^{-3}) was calculated such that the initial total organic aerosol mass matched the $\Delta OA/\Delta CO_2$ emission ratio from Akagi et al. (2012). The evolution of the aerosol size distribution with time was simulated by ASP v2.1 using a center-moving sectional size distribution with 10 bins, 8 bins for particles with volume-equivalent spherical diameters between 0.05 and 2.0 µm, one for particles with diameters smaller than 0.05 µm, and one for particles with diameters greater than 2 µm.

Photolysis rates were calculated offline using TUV v5.0 (Madronich and Flocke, 1998) as noted in Sect. 2.2 above. The smoke aerosols were assumed to dilute with time according to the three dilution rates derived above (see Fig. 3). In the TUV simulations, we assumed no clouds and an initial AOD of 8.0 at 330 nm (consistent with the ASP v2.1 calculated initial extinction coefficient and the assumed plume thickness of 1 km), which decreases due to dilution assuming a background concentration of ~ 0, as well as a constant single scattering albedo of 0.9 (based on the review of AERONET biomass burning smoke optical property retrievals by Reid et al., 2005a). We also assumed initial plume and background concentrations of the trace gases NO_2 (initial 295 ppbv, background 0 ppbv) and SO_2 (initial 50.9 ppbv, background 0 ppbv), as these species can also absorb ultraviolet and visible (UV-VIS) light and thus can impact photolysis rates. For the photolysis rate calculations only, O_3 was assumed to be 0 initially and increased after 15 min to a constant value of 100 ppbv to account for the observed formation of O_3 within the smoke plume. The overhead ozone column was assumed to be 278 Dobson Units (DU), based on the average of values from the Ozone Monitoring Instrument (OMI) for 11/16/2009 (276 DU) and 11/18/2009 (280 DU) (accessed through http://jwocky.gsfc.nasa.gov/teacher/ozone_overhead.html on June 2012, now at: http://ozoneaq.gsfc.nasa.gov/tools/ozonemap/ozone_overhead). The surface albedo was assumed to be 0.035 based on the GEOS-Chem data file for the $0.5^\circ \times 0.667^\circ$ North American grid for November 1985, which is in turn based on data from the Total Ozone Mapping Spectrometer (TOMS). Photolysis rates were calculated for three altitudes: just above the plume (i.e., at 2.1 km altitude), near the

ACPD
14, 32427–32489, 2014

middle of the plume (1.6 km), and near the bottom of the plume (1.1 km). This, combined with the three dilution rates, gave nine estimates of photolysis rates vs. time. The nine values for the NO_2 photolysis rate (J_{NO_2}) were compared with the clear sky (no aerosol) case in Fig. 4. In the middle of the plume (1.6 km), J_{NO_2} was reduced from an initial clear-sky value of $9 \times 10^{-3}\,s^{-1}$ to an initial value of $2 \times 10^{-3}\,s^{-1}$. However, by 15 min after emission J_{NO_2} in the middle of the plume increased to 6–$8.5 \times 10^{-3}\,s^{-1}$ depending on the dilution rate, showing that the plume reduced photolysis rates by 5–33 % after the initial, rapid dilution of the plume. J_{NO_2} was slightly enhanced above the plume (initially $1.1 \times 10^{-3}\,s^{-1}$) over the clear sky value, and the photolysis rates were lowest in the bottom of the plume. As expected, the impact of the plume was larger for lower dilution rates, but the difference between the different dilution rates was largest for the bottom of the plume.

5.2 ASP results with no unidentified SVOC chemistry

We first ran ASP assuming the unidentified SVOCs emitted by the fire are unreactive. Deficiencies in these simulations provide information on what the average chemistry of the unidentified SVOCs needs to be in order to explain the observations.

Figure 5 shows the ASP v2.1 results and Akagi et al. (2012) observations for the enhancement ratios (EnR, mol mol^{-1}) of O_3 and PAN in the Williams Fire smoke plume vs. time after emissions. The EnR is defined as the ratio of the enhancement of a species X within the smoke plume ($\Delta X = C_x - C_x^a$, Akagi et al., 2011) to the enhancement of a less reactive species, such as CO_2 or CO. We can see that the range of dilution rates and photolysis rates simulated for this case capture the general rate of the secondary formation of O_3 and PAN, but ASP v2.1 appears to be overestimating the rate of formation of these compounds. This is in contrast to Alvarado and Prinn (2009), who found that ASP v1.0 dramatically underestimated the much faster O_3 formation in the Timbavati savannah fire smoke plume.

ACPD
14, 32427–32489, 2014

The ASP v2.1 "average" value (i.e., the best-fit dilution combined with the middle of the plume photolysis rates, plotted as a solid black line in Fig. 5) at 4.5 h for $\Delta O_3/\Delta CO$ is 0.116 mol mol^{-1} which is within the uncertainty associated with the average value measured for the Williams Fire (0.095 ± 0.022). This overestimate is similar to the positive bias (~ 25 %) of the SAPRC-07 mechanism vs. the EPA smog chamber for low ROG/NO_x (< 20 ppb C/ppb N) ratios when aromatics are not part of the surrogate. As aromatics are a minor constituent in biomass burning smoke, and the ROG/NO_x ratio for savannah/scrubland fires like the Williams Fire (without including unidentified species) is ~ 10 ppb C/ppb N, we would expect the mechanism in ASP v2.1 to show a similar positive bias. ASP v2.1 predicts an "average" value of $\Delta PAN/\Delta CO$ of 0.012 at 4.5 h downwind, 68 % larger than the observed value of 0.0072 ± 0.0017.

Figure 6 shows the ASP v2.1 results and observations for $\Delta NO_x/\Delta CO_2$ and $\Delta C_2H_4/\Delta CO$ vs. time. Figure 6a shows that the $\Delta NO_x/\Delta CO_2$ values 2–5 h after emission are correctly simulated by ASP v2.1, with the "average" ASP case EnR of 3.4×10^{-4} matching the observed value of $4.6 \pm 2.3 \times 10^{-4}$. However, the observations show a faster rate of decay in the first two hours after emission than is seen in the model results. Figure 6b shows that the decay of C_2H_4 is also well matched by the model results, suggesting that the modeled OH is similar to the actual OH concentrations. This can also be seen by comparing the modeled OH concentration for the "average" case (5.3×10^6 molecules cm^{-3}) to that derived by Akagi et al. (2012) using the observed decay of C_2H_4 ($5.27 \pm 0.97 \times 10^6$ molecules cm^{-3}). This is again in contrast with Alvarado and Prinn (2009), who found that ASP underestimated the observed OH radical concentrations for the Timbavati smoke plume (1.7×10^7 molecules cm^{-3}, Hobbs et al., 2003).

We can explore this contrast further by looking at the rate of loss of HONO in the smoke plume, shown in Fig. 7. Note that unlike the previous figures, Fig. 7 only shows the first hour after emission as the observations showed no detectable HONO further downwind. As noted in Sect. 1, to explain the underestimate of O_3 and OH in the Timbavati fire, Alvarado and Prinn (2009) posited that a heterogeneous reaction of NO_2

ACPD
14, 32427–32489, 2014

to make HONO and HNO_3 was taking place in that plume. However, the O_3 and OH results for the Williams Fire show no evidence of this chemistry, and the HONO decay seen in Fig. 7 also shows little evidence for a secondary source of HONO except for a few points within the first 12 min after emission that have more HONO than is predicted by the model. While explaining the discrepancy between the Williams and Timbavati results is beyond the scope of this paper, we note that the Timbavati fire took place closer to the equator (24° S vs. 35° N) and earlier in the year (7 September vs. 17 November) than the Williams Fire, and that the relative humidity was slightly higher as well (45.0 vs. 15.7 %). All of these differences would tend to increase photolysis rates and the formation of OH. In addition, the higher actinic flux and RH in Timbavati may have increased the speed of reactions for forming HONO from NO_2 that are not included in standard chemical mechanisms, either via aqueous chemistry (Jacob et al., 2000), sunlight-activated humic acid surfaces (Stemmler et al., 2006, 2007), or photoexcited NO_2 reacting with H_2O (Ensberg et al., 2010). Though we find no evidence for secondary HONO production in the Williams Fire data, this does not preclude that some HONO was made, but remained below the AFTIR detection limit as the plume diluted.

Figure 8 shows the ASP results for the aldehydes such as HCHO and glycoaldehyde ($HCOCH_2OH$), and the organic acids as well as formic acid (HCOOH) and acetic acid (CH_3COOH) within the Williams Fire in terms of EnRs to CO. We can see that ASP generally underestimates the formation of these species. Part of this underestimate may be due to errors in the chemical mechanism for known precursor compounds, as was seen for HCHO in the smog chamber results in Fig. 1b, but neglecting the chemistry of the SVOCs and their ability to form these smaller organic compounds is also likely responsible for this underestimate.

5.3 OH reaction rate and fragmentation probability of the unidentified SVOCs

Here we evaluate the ability of the parameters from the original VBS paper of Robinson et al. (2007), a study of SOA formation in wood smoke by Grieshop et al. (2009a, b),

ACPD
14, 32427–32489, 2014

and the implementation of the VBS scheme into WRF-Chem by Ahmadov et al. (2012) to simulate the observed evolution of OA in the Williams Fire plume. Table 5 shows the values for the parameters in Reactions (R3) and (R4) that define these various SVOC mechanisms.

Figure 9 shows the modeled OA enhancement ratios ($\Delta OA/\Delta CO_2$, $g\,g^{-1}$) at 4.5 h downwind using the parameters listed in Table 5 in addition to the observed average OA enhancement ratio and the modeled OA enhancement ratio for the case where the chemistry of the unidentified SVOCs is not included (see Sect. 5.2). When SVOC chemistry was not included, some of the original OA evaporated into the gas phase as the plume diluted, and as there was no chemistry to make these SVOC species less volatile, they stayed in the gas phase leading to a net decrease in $\Delta OA/\Delta CO_2$ with time. However, the modeled decrease without SVOC chemistry is larger (but still within the error bars) of the decrease that was reported by Akagi et al. (2012). In addition, the assumption that the SVOCs do not react is unrealistic – as large multi-functional organic compounds, they should have a relatively fast reaction rate with OH (see below).

Figure 9 also shows that the SVOC mechanisms of Robinson et al. (2007) and Grieshop et al. (2009a, b) overestimated the OA downwind by a factor of 3.1 and 7.2, respectively. This is primarily due to their relatively large values for k_{OH}. For the Grieshop et al. (2009a, b) case, the overestimation is also partially due to the large increase in mass (μ) and decrease in volatility (n) for each OH reaction. The scheme of Ahmadov et al. (2012), with $k_{OH} = 10^{-11}\,cm^3\,molecule^{-1}\,s^{-1}$, was closest to the observations, with an overestimate of a factor of 1.9. One approach to further reduce this remaining overestimation would be to reduce k_{OH} even further. However, it seems unlikely that the average OH reaction rate of the unidentified SVOC species would be less than $10^{-11}\,cm^3\,molecule^{-1}\,s^{-1}$, as this is close to the reaction rate for large alkanes ($k_{OH}(298\,K) = 1.1 \times 10^{-11}\,cm^3\,molecule^{-1}\,s^{-1}$, Goliff et al., 2013) and the presence of other functional groups (double bonds, aldehydes) would be expected to result in even higher reaction rates. For example, α-pinene has a $k_{OH}(298\,K)$ of

ACPD
14, 32427–32489, 2014

5.0×10^{-11} cm^3 molecule^{-1} s^{-1} (Goliff et al., 2013), and other monoterpenes can have even faster reaction rates with OH. Thus, we think a more likely explanation for the remaining overestimate is that a substantial fraction of the SVOC and OH reactions resulted in the fragmentation of the primary SVOC into more volatile compounds, as in the 2D-VBS schemes of Jimenez et al. (2009) and Donahue et al. (2011).

Figure 9 shows that a k_{OH} of 10^{-11} cm^3 molecule^{-1} s^{-1} and a fragmentation probability of 50 % (the "Half Fragmentation" case, see Table 5) provided a reasonably good match with the observed $\Delta OA/\Delta CO_2$ 4.5 h downwind in the smoke plume (3.1×10^{-3} vs. the observed value of $2.83 \pm 1.02 \times 10^{-3}$). Here we assumed that the SVOC fragmented into a small VOC and another, more volatile, SVOC, as in Reactions (R3) and (R4). While this is a relatively large fragmentation probability, we note that it seems reasonable given the likely complex and multifunctional nature of the unidentified SVOCs in a biomass burning smoke plume.

This fragmentation of the SVOCs after reaction with OH could also help to explain the underestimate of aldehydes and organic acids seen in Sect. 5.2 when SVOC chemistry was neglected. For example, Fig. 10 shows the ASP modeled EnR of acetic acid when we assumed that the VOC fragment produced in Reaction (R4) is acetic acid. This provided a remarkably good match with the observed acetic acid formation, providing additional evidence to support the fragmentation hypothesis. While we are not claiming to have proven this is the source of the missing acetic acid, we note that the fragmentation hypothesis is thus consistent with the initial underestimate of the secondary formation of aldehydes and organic acids in ASP v2.1. In addition, there is some evidence from biomass burning plume observations that the formation of acetic acid and OA are inversely correlated with each other. In the Yucatan plume studied by Yokelson et al. (2009), a large amount of SOA was formed, but acetic acid did not increase downwind, while in the Williams Fire, acetic acid increased, but OA did not. Thus, the limited amount of relevant airborne data in BB plumes is so far consistent with the idea that the branching between functionalization and fragmentation in BB plumes

ACPD
14, 32427–32489, 2014

is variable and future work should identify what environmental and combustion factors determine this variability.

An additional potential explanation for the SOA overestimate observed when the schemes of the Robinson et al. (2007), Grieshop et al. (2009a, b), and Ahmadov et al. (2012) were used is that the OA was becoming more viscous and "glassy" with time (i.e., the particles had a lower bulk diffusivity), thereby reducing the amount of quasi-liquid OA for SVOC compounds to dissolve into (e.g., Kidd et al., 2014; Zaveri et al., 2014). There has been some recent evidence for this process occurring in smoke plumes from biomass burning in the western US (A. Sedlacek, personal communication, March 2014). ASP v2.1 is not able to examine this possibility in detail, but we do note that while the formation of "glassy" OA would reduce SOA formation, it likely would not increase the formation of aldehydes or organic acids as in the fragmentation hypothesis.

5.4 HO_x and NO_x chemistry of the unidentified SVOCs

Section 5.2 showed that an SVOC mechanism following Reaction (R2) with a k_{OH} of 10^{-11} cm^3 molecule^{-1} s^{-1} and a fragmentation probability α of 0.5 (the "Half Fragmentation" scheme in Table 5) could explain the observed evolution of OA in the Williams Fire. However, neglecting the regeneration of HO_x and reaction of the peroxy radical with NO, as in Reaction (R2), can lead to substantial underestimates of OH in the concentrated smoke plumes. This is because including Reaction (R2) in ASP leads to a loss of OH with no corresponding regeneration of HO_2.

For example, Fig. 11 shows that using the "Half Fragmentation" scheme reduced the ASP v2.1 estimates of the enhancement ratios of O_3 and PAN downwind by 32 and 67 %, respectively (for the "average" case), while Fig. 12 shows that it increased the ASP v2.1 estimates of C_2H_4 and NO_x downwind by 50 % and a factor of 3.3, respectively. The new O_3 and PAN estimates are more consistent with the observations – the overestimate of PAN seen with the unidentified SVOC chemistry neglected in Sect. 5.2 has disappeared – but the large overestimate of NO_x (i.e., underestimate of NO_x loss in

ACPD
14, 32427–32489, 2014

the plume presumably due to missing organic nitrogen formation) is a serious problem. While this underestimate of NO_x loss reduces the amount of O_3 and PAN formed within five hours after emission, it would lead to large overestimates of the impact of biomass burning plumes on O_3 and PAN formation further downwind.

In addition, the chemistry of Reaction (R2) is unrealistic, in that it implies a total loss of OH and no effect of the SVOC oxidation on NO_x. One approach for addressing the first concern is to artificially regenerate the OH by simply adding it as an additional product to Reaction (R2). While this makes sense as a "first do no harm" modeling approach to keep the gas-phase results the same regardless of the SVOC scheme, it is equally unrealistic, as it assumes that the SVOCs are oxidized without having any impact on NO_x or HO_x.

We prefer to approach this problem by recognizing that SVOCs are going to have impacts on the HO_x and NO_x radical budgets just like any other organic species, and that this chemistry can be approximated via Reactions (R3) and (R4). Including this more realistic, yet still simplified, chemistry allows ASP to simultaneously simulate the observed changes in OA and O_3 while still making reasonable, chemically plausible assumptions about the chemistry of the unidentified SVOCs emitted by the fire.

Our approach thus used the observations of OA, O_3, PAN, NO_x, and C_2H_4 in the Williams Fire as constraints on β and δ, the amount of NO_2 and HO_2 produced in Reaction (R4), respectively, while assuming that $\chi = 1$ throughout. For the Williams Fire, we know from the above results that we want the optimized SVOC chemistry to (a) increase O_3, PAN, and OA formation as little as possible, (b) increase the loss of NO_x, either through organic nitrate formation or increased OH concentrations, and (c) increase the OH concentration, thereby increasing C_2H_4 loss. We found that using the parameters for large alkanes from RACM2 ($\delta = 0.63$ and $\beta = 0.74$) generally produced too much O_3 and PAN and too little OH, but did a reasonable job for NO_x loss. However, attempts to increase OH by increasing δ led to too much O_3 formation except for unrealistically low values of β (~ 0.1). Thus we set $\delta = 0.6$ and reduced β to 0.5, implying that 1.1 O_3 is formed per molecule of SVOC reacted. These parameters (arrived at by

ACPD
14, 32427–32489, 2014

trial and error) appear to give the best balance of reducing modeled NO_x and C_2H_4 mixing ratios while minimizing the increase in O_3, PAN, and OA. The following section discusses the ASP v2.1 model results for the Williams Fire smoke plume using these parameters in detail. Note that while slightly different, more precise parameters might provide a slightly better match with observation, our goal here is not to derive exact best-fit parameters, but rather to roughly classify the average chemistry of the SVOCs in the Williams Fire smoke plume, both for modeling this fire and for future comparisons with other smoke plumes.

5.5 Results with optimized SVOC chemistry

Figure 9 shows the $\Delta OA/\Delta CO_2$ 4.5 h downwind in the smoke plume using the optimized SVOC chemistry discussed in Sect. 5.4. The "average" model case $\Delta OA/\Delta CO_2$ is 3.5×10^{-3} ($g\,g^{-1}$), within the uncertainty of the observed value of $2.83 \pm 1.02 \times 10^{-3}$.

Figure 13 shows the enhancement ratios of O_3 and PAN for the optimized SVOC chemistry, and Fig. 14 shows the results for NO_x and C_2H_4. The O_3 results are very similar to those from Sect. 5.2 (where SVOC chemistry was not included in the model), while the PAN results are slightly lower (and closer to the observed values) than in that case. In the ASP "average" case $\Delta O_3/\Delta CO$ is 0.119 at 4.5 h downwind, about 25 % larger than the observed value of 0.095 ± 0.022, while the $\Delta PAN/\Delta CO$ is now 0.0098 at 4.5 h downwind, about 36 % larger than the observed value of 0.0072 ± 0.0017. However, the O_3 and PAN values are reasonably close given the uncertainties in the concentrations and in the estimated smoke ages for the observations.

The NO_x results were much improved from the "half frag" case in Sect. 5.4, with the "average" ASP case $\Delta NO_x/\Delta CO_2$ of 9.6×10^{-4} being below the mean observed value of $4.6 \pm 2.3 \times 10^{-3}$, but consistent with the error bars of the individual samples as shown in Fig. 14. We could attempt to get a closer match by increasing β, but at the cost of increases in the modeled O_3, PAN, and OA formation. The decay of C_2H_4 is also better modeled than in the "Half Fragmentation" case, but the results

ACPD
14, 32427–32489, 2014

suggest OH was still underestimated in the model. The modeled OH concentration for the "average" case is now 3.2×10^6 molecules cm^{-3}, below the observed value of $5.27 \pm 0.97 \times 10^6$ molecules cm^{-3}, but attempts to increase OH by increasing δ would increase O_3, PAN, and OA.

6 Conclusions

We have used version 2.1 of the ASP model, which includes extensive updates to the gas-phase chemistry and SOA formation modules, to simulate the near-source chemistry within the smoke plume from the Williams Fire, as sampled by Akagi et al. (2012). We find that the assumptions made about the chemistry of the unidentified SVOCs emitted by the fire have a large impact on the simulated secondary formation of O_3, PAN, and OA within the plume. We showed that reasonable assumptions about the chemistry of the unidentified SVOCs can successfully simulate the observations within the uncertainties of the measurements, the estimated smoke ages of the samples, the plume dilution rate, and the vertical location of the samples in the plume. For the Williams Fire, these assumptions were: (1) a reaction rate constant with OH of $\sim 10^{-11}$ cm^3 s^{-1}, (2) a significant fraction (~ 50 %) of the $RO_2 + NO$ reaction resulted in fragmentation, rather than functionalization, (3) ~ 1.1 molecules of O_3 were formed for every molecule of SVOC that reacts; and (4) 60 % of the OH that reacted with the SVOC was regenerated as HO_2 by the $RO_2 + NO$ reaction, which implied (5) that 50 % of the NO that reacted with the SVOC peroxy radicals was lost, likely due to to organic nitrate formation.

The method used in this study can provide a way of classifying different smoke plume observations in terms of the average chemistry of their unidentified SVOCs. Similar studies of other young biomass burning plumes would allow us to see how the chemistry of the unidentified SVOCs varies with fuel type, combustion efficiency, and other environmental parameters, providing an additional constraint on the reactivities of the unidentified SVOCs. These constraints could then provide more insight into the for-

ACPD
14, 32427–32489, 2014

mation of O_3, PAN, and OA in young biomass burning smoke plumes and serve as the basis of parameterizing this process for regional or global scale models. Future field experiments, focused on quasi-Lagrangian sampling of biomass burning smoke plumes, may also provide data beyond that available for the Williams Fire that will increase our understanding of the chemistry of these plumes. These include (a) observations of changes in particle size distribution to test model simulations of condensational growth, coagulation, and new particle formation, (b) observations of a larger suite of NO_y species, such as $HNO_{3(g)}$, peroxy nitrates, and alkyl nitrates, for use in studying and constraining the transformations of reactive nitrogen, (c) measurements of organic aerosol viscosity and mixing state with black carbon and inorganic aerosols, and (d) more detailed measurements of the currently unidentified organic species present in the smoke plumes.

The Supplement related to this article is available online at doi:10.5194/acpd-14-32427-2014-supplement.

Acknowledgements. This modeling work was funded by NSF grant number AGS-1144165 to M. J. Alvarado and C. R. Lonsdale of Atmospheric and Environmental Research (AER) and RY of the University of Montana. Original sampling of the Williams Fire was funded primarily by the Strategic Environmental Research and Development Program (SERDP) projects SI-1648 and SI-1649 and partially by NSF grants ATM-0513055 and ATM-0936321.

References

Ahmadov, R., McKeen, S. A., Robinson, A. L., Bahreini, R., Middlebrook, A. M., de Gouw, J. A., Meagher, J., Hsie, E.-Y., Edgerton, E., Shaw, S., and Trainer, M.: A volatility basis set model for summertime secondary organic aerosols over the eastern United States in 2006, J. Geophys. Res., 117, 2156–2202, 2012.

ACPD
14, 32427–32489, 2014

Akagi, S. K., Yokelson, R. J., Wiedinmyer, C., Alvarado, M. J., Reid, J. S., Karl, T., Crounse, J. D., and Wennberg, P. O.: Emission factors for open and domestic biomass burning for use in atmospheric models, Atmos. Chem. Phys., 11, 4039–4072, doi:10.5194/acp-11-4039-2011, 2011.

Akagi, S. K., Craven, J. S., Taylor, J. W., McMeeking, G. R., Yokelson, R. J., Burling, I. R., Urbanski, S. P., Wold, C. E., Seinfeld, J. H., Coe, H., Alvarado, M. J., and Weise, D. R.: Evolution of trace gases and particles emitted by a chaparral fire in California, Atmos. Chem. Phys., 12, 1397–1421, doi:10.5194/acp-12-1397-2012, 2012.

Akagi, S. K., Yokelson, R. J., Burling, I. R., Meinardi, S., Simpson, I., Blake, D. R., McMeeking, G. R., Sullivan, A., Lee, T., Kreidenweis, S., Urbanski, S., Reardon, J., Griffith, D. W. T., Johnson, T. J., and Weise, D. R.: Measurements of reactive trace gases and variable O_3 formation rates in some South Carolina biomass burning plumes, Atmos. Chem. Phys., 13, 1141–1165, doi:10.5194/acp-13-1141-2013, 2013.

Allan, J. D., Delia, A. E., Coe, H., Bower, K. N., Alfarra, M. R., Jimenez, J. L., Middlebrook, A. M., Drewnick, F., Onasch, T. B., Canagaratna, M. R., Jayne, J. T., and Worshop, D. R.: A generalized method for the extraction of chemically resolved mass spectra from Aerodyne aerosol mass spectrometer data, J. Aerosol Sci., 35, 909–922, 2004.

Alvarado, M. J.: Formation of Ozone and Growth of Aerosols in Young Smoke Plumes from Biomass Burning, Ph.D. thesis, Massachusetts Institute of Technology, Cambridge, MA, USA, 324 pp., available at: http://globalchange.mit.edu/files/document/Alvarado_PhD_08.pdf, last access: December 11, 2014, 2008.

Alvarado, M. J. and Prinn, R. G.: Formation of ozone and growth of aerosols in young smoke plumes from biomass burning, Part 1: Lagrangian parcel studies, J. Geophys. Res., 114, D09306, doi:10.1029/2008JD011144, 2009.

Alvarado, M. J., Wang, C., and Prinn, R. G.: Formation of ozone and growth of aerosols in young smoke plumes from biomass burning, Part 2: 3-D Eulerian studies, J. Geophys. Res., 114, D09307, doi:10.1029/2008JD011186, 2009.

Alvarado, M. J., Logan, J. A., Mao, J., Apel, E., Riemer, D., Blake, D., Cohen, R. C., Min, K.-E., Perring, A. E., Browne, E. C., Wooldridge, P. J., Diskin, G. S., Sachse, G. W., Fuelberg, H., Sessions, W. R., Harrigan, D. L., Huey, G., Liao, J., Case-Hanks, A., Jimenez, J. L., Cubison, M. J., Vay, S. A., Weinheimer, A. J., Knapp, D. J., Montzka, D. D., Flocke, F. M., Pollack, I. B., Wennberg, P. O., Kurten, A., Crounse, J., Clair, J. M. St., Wisthaler, A., Mikoviny, T., Yantosca, R. M., Carouge, C. C., and Le Sager, P.: Nitrogen oxides and PAN in plumes from

ACPD
14, 32427–32489, 2014

boreal fires during ARCTAS-B and their impact on ozone: an integrated analysis of aircraft and satellite observations, Atmos. Chem. Phys., 10, 9739–9760, doi:10.5194/acp-10-9739-2010, 2010.

Alvarado, M. J., Cady-Pereira, K. E., Xiao, Y., Millet, D. B., and Payne, V. H.: Emission ratios for ammonia and formic acid and observations of Peroxy Acetyl Nitrate (PAN) in biomass burning smoke as seen by the Tropospheric Emission Spectrometer (TES), Atmosphere, 2, 633–654, doi:10.3390/atmos2040633, 2011.

Andreae, M. O. and Merlet, P.: Emission of trace gases and aerosols from biomass burning, Global Biogeochem. Cy., 15, 955–966, 2001.

Andreae, M. O., Anderson, B. E., Blake, D. R., Bradshaw, J. D. Collins, J. E., Gregory, G. L., Sachse, G. W., and Shipham, M. C.: Influence of plumes from biomass burning on atmospheric chemistry over the equatorial and tropical South Atlantic during CITE 3, J. Geophys. Res., 99, 12793–12808, doi:10.1029/94JD00263, 1994.

Arnold, S. R., Emmons, L. K., Monks, S. A., Law, K. S., Ridley, D. A., Turquety, S., Tilmes, S., Thomas, J. L., Bouarar, I., Flemming, J., Huijnen, V., Mao, J., Duncan, B. N., Steenrod, S., Yoshida, Y., Langner, J., and Long, Y.: Biomass burning influence on high latitude tropospheric ozone and reactive nitrogen in summer 2008: a multi-model analysis based on POLMIP simulations, Atmos. Chem. Phys. Discuss., 14, 24573–24621, doi:10.5194/acpd-14-24573-2014, 2014.

Atkinson, R., Baulch, D. L., Cox, R. A., Crowley, J. N., Hampson, R. F., Hynes, R. G., Jenkin, M. E., Rossi, M. J., and Troe, J.: Evaluated kinetic and photochemical data for atmospheric chemistry: Volume I - gas phase reactions of O_x, HO_x, NO_x and SO_x species, Atmos. Chem. Phys., 4, 1461–1738, doi:10.5194/acp-4-1461-2004, 2004.

Baylon, P., Jaffe, D. A., Wigder, N. L., Gao, H., and Hee, J.: Ozone enhancement in Western US wildfire plumes at the Mt. Bachelor Observatory: the role of NO_x, Atmos. Environ., in press, 2014.

Beswick, K. M., Gallagher, M. W., Webb, A. R., Norton, E. G., and Perry, F.: Application of the Aventech AIMMS20AQ airborne probe for turbulence measurements during the Convective Storm Initiation Project, Atmos. Chem. Phys., 8, 5449–5463, doi:10.5194/acp-8-5449-2008, 2008.

Bey, I., Jacob, D. J., Yantosca, R. M., Logan, J. A., Field, B. D., Fiore, A. M., Li, Q., Liu, H. Y., Mickley, L. J., and Schultz, M. G.: Global modeling of tropospheric chemistry with assimilated meteorology: model description and evaluation, J. Geophys. Res., 106, 23073–23095, 2001.

ACPD
14, 32427–32489, 2014

Bloss, C., Wagner, V., Jenkin, M. E., Volkamer, R., Bloss, W. J., Lee, J. D., Heard, D. E., Wirtz, K., Martin-Reviejo, M., Rea, G., Wenger, J. C., and Pilling, M. J.: Development of a detailed chemical mechanism (MCMv3.1) for the atmospheric oxidation of aromatic hydrocarbons, Atmos. Chem. Phys., 5, 641–664, doi:10.5194/acp-5-641-2005, 2005.

Bowman, F. M. and Seinfeld, J. H.: Fundamental basis of incremental reactivities of organics in ozone formation in VOC/NO_x mixtures, Atmos. Environ., 28, 3359–3368, 1994a.

Bowman, F. M. and Seinfeld, J. H.: Ozone productivity of atmospheric organics, J. Geophys. Res., 99, 5309–5324, 1994b.

Canagaratna, M. R., Jayne, J. T., Jimenez, J. L., Allan, J. D., Alfarra, M. R., Zhang, Q., Onasch, T. B., Drewnick, F., Coe, H., Middlebrook, A., Delia, A., Williams, L. R., Trimborn, A. M., Northway, M. J., DeCarlo, P. F., Kolb, C. E., Davidovits, P., and Worsnop, D. R.: Chemical and microphysical characterization of ambient aerosols with the Aerodyne aerosol mass spectrometer, edited by: Viggiano, A., Mass Spectrom. Rev., 26, 185–222, 2007.

Capes, G., Johnson, B., McFiggans, G., Williams, P. I., Haywood, J., and Coe, H.: Aging of biomass burning aerosols over West Africa: aircraft measurements of chemical composition, microphysical properties, and emission ratios, J. Geophys. Res., 113, D00C15, doi:10.1029/2008JD009845, 2008.

Carter, W. P.: Development of ozone reactivity scales for volatile organic compounds, Air and Waste, 44, 881–899, 1994.

Carter, W. P.: Documentation of the SAPRC-99 chemical mechanism for VOC reactivity assessment, Tech. rep., Draft report to the California Air Resources Board, Contracts 92-329 and 95-308, 2000.

Carter, W., Luo, D., Malkina, I., and Pierce, J.: Environmental chamber studies of atmospheric reactivities of volatile organic compounds: effects of varying ROG surrogate and NO_x, Tech. rep., Final Report to Coordinating Research Council, Inc., Project ME-9, California Air Resources Board, Contract A032-0692, and South Coast Air Quality Management District, Contract C91323, available at: http://www.cert.ucr.edu/carter/absts.htm#rct2rpt, 1995.

Carter, W. P., Cocker, I., David, R., Fitz, D. R., Malkina, I. L., Bumiller, K., Sauer, C. G., Pisano, J. T., Bufalino, C., and Song, C.: A new environmental chamber for evaluation of gas-phase chemical mechanisms and secondary aerosol formation, Atmos. Environ., 39, 7768–7788, 2005.

Carter, W. P. L.: Mechanism and updated ozone reactivity scales, Report to the California Air Resources Board, Contracts No. 03-318, 06–408, and 07-730, 27 January, 2010.

ACPD
14, 32427–32489, 2014

Christian, T., Kleiss, B., Yokelson, R., Holzinger, R., Crutzen, P., Hao, W., Saharjo, B., and Ward, D.: Comprehensive laboratory measurements of biomas-burning emissions: 1. Emissions from Indonesian, African, and other fuels, J. Geophys. Res., 108, D23, 4719, doi:doi:10.1029/2003JD003704, 2003.

Crounse, J. D., Paulot, F., Kjaergaard, H. G., and Wennberg, P. O.: Peroxy radical isomerization in the oxidation of isoprene, Phys. Chem. Chem. Phys., 13, 13607–13613, 2011.

Crounse, J. D., Knap, H. C., Ørnsø, K. B., Jørgensen, S., Paulot, F., Kjaergaard, H. G., and Wennberg, P. O.: Atmospheric fate of methacrolein. 1. Peroxy radical isomerization following addition of OH and O_2, J. Phys. Chem. A, 116, 5756–5762, 2012.

Crutzen, P. J. and Andreae, M. O.: Biomass burning in the tropics: impact on atmospheric chemistry and biogeochemical cycles, Science, 250, 1669–1678, 1990.

Donahue, N. M., Epstein, S. A., Pandis, S. N., and Robinson, A. L.: A two-dimensional volatility basis set: 1. organic-aerosol mixing thermodynamics, Atmos. Chem. Phys., 11, 3303–3318, doi:10.5194/acp-11-3303-2011, 2011.

Drewnick, F., Schwab, J. J., Hogrefe, O., Peters, S., Husain, L., Diamond, D., Weber, R., and Demerjian, K. L.: Intercomparison and evaluation of four semi-continuous $PM_{2.5}$ sulfate instruments, Atmos. Environ., 37, 3335–3350, 2003.

Drewnick, F., Hings, S. S., DeCarlo, P., Jayne, J. T., Gonin, M., Fuhrer, K., Weimer, S., Jimenez, J. L., Demerjian, K. L., Borrmann, S., and Worsnop, D. R.: A new Time-of-Flight Aerosol Mass Spectrometer (TOF-AMS) – instrument description and first field deployment, Aerosol Sci. Tech., 39, 637–658, 2005.

Dzepina, K., Volkamer, R. M., Madronich, S., Tulet, P., Ulbrich, I. M., Zhang, Q., Cappa, C. D., Ziemann, P. J., and Jimenez, J. L.: Evaluation of recently-proposed secondary organic aerosol models for a case study in Mexico City, Atmos. Chem. Phys., 9, 5681–5709, doi:10.5194/acp-9-5681-2009, 2009.

Ensberg, J. J., Carreras-Sospedra, M., and Dabdub, D.: Impacts of electronically photo-excited NO_2 on air pollution in the South Coast Air Basin of California, Atmos. Chem. Phys., 10, 1171–1181, doi:10.5194/acp-10-1171-2010, 2010.

Fischer, E. V., Jaffe, D. A., Reidmiller, D. R., and Jaeglé, L.: Meteorological controls on observed peroxyacetyl nitrate at Mount Bachelor during the spring of 2008, J. Geophys. Res., 115, D03302, doi:10.1029/2009JD012776, 2010.

Fischer, E. V., Jacob, D. J., Yantosca, R. M., Sulprizio, M. P., Millet, D. B., Mao, J., Paulot, F., Singh, H. B., Roiger, A., Ries, L., Talbot, R. W., Dzepina, K., and Pandey Deolal, S.: Atmo-

ACPD
14, 32427–32489, 2014

spheric peroxyacetyl nitrate (PAN): a global budget and source attribution, Atmos. Chem. Phys., 14, 2679–2698, doi:10.5194/acp-14-2679-2014, 2014.
Fountoukis, C. and Nenes, A.: ISORROPIA II: a computationally efficient thermodynamic equilibrium model for K^+–Ca^{2+}–Mg^{2+}–NH_4^+–Na^+–SO_4^{2-}–NO_3^-–Cl^-–H_2O aerosols, Atmos. Chem. Phys., 7, 4639–4659, doi:10.5194/acp-7-4639-2007, 2007.
Goliff, W. S., Stockwell, W. R., and Lawson, C. V.: The regional atmospheric chemistry mechanism, version 2, Atmos. Environ., 68, 174–185, 2013.
Goode, J. G., Yokelson, R. J., Ward, D. E., Susott, R. A., Babbitt, R. E., Davies, M. A., and Hao, W. M.: Measurements of excess O_3, CO_2, CO, CH_4, C_2H_4, C_2H_2, HCN, NO, NH_3, HCOOH, CH_3COOH, HCHO and CH_3OH in 1997 Alaskan biomass burning plumes by airborne fourier transform infrared spectroscopy (AFTIR), J. Geophys. Res., 105, 22147–22166, 2000.
Grieshop, A. P., Logue, J. M., Donahue, N. M., and Robinson, A. L.: Laboratory investigation of photochemical oxidation of organic aerosol from wood fires 1: measurement and simulation of organic aerosol evolution, Atmos. Chem. Phys., 9, 1263–1277, doi:10.5194/acp-9-1263-2009, 2009a.
Grieshop, A. P., Donahue, N. M., and Robinson, A. L.: Laboratory investigation of photochemical oxidation of organic aerosol from wood fires 2: analysis of aerosol mass spectrometer data, Atmos. Chem. Phys., 9, 2227–2240, doi:10.5194/acp-9-2227-2009, 2009b.
Griffin, R. J., Nguyen, K., Dabdub, K. D., and Seinfeld, J. H.: A coupled hydrophobic-hydrophilic model for predicting secondary organic aerosol formation, J. Atmos. Chem., 44, 171–190, 2003.
Griffin, R. J., Dabdub, D., and Seinfeld, J. H.: Development and initial evaluation of a dynamic species-resolved model for the gas phase chemistry and size-resolved gas/particle partitioning associated with secondary organic aerosol formation, J. Geophys. Res., 110, D05304, doi:10.1029/2004JD005219, 2005.
Heilman, W. E., Liu, Y., Urbanski, S., Kovalev, V., Mickler, R.: Wildland fire emissions, carbon, and climate: plume rise, atmospheric transport, and chemistry processes, For. Ecol. Manage., 317, 70–79, doi:10.1016/j.foreco.2013.02.001, available at: http://www.treesearch.fs.fed.us/pubs/45645, 2014.
Hennigan, C. J., Miracolo, M. A., Engelhart, G. J., May, A. A., Presto, A. A., Lee, T., Sullivan, A. P., McMeeking, G. R., Coe, H., Wold, C. E., Hao, W.-M., Gilman, J. B., Kuster, W. C., de Gouw, J., Schichtel, B. A., Collett Jr., J. L., Kreidenweis, S. M., and Robinson, A. L.:

ACPD
14, 32427–32489, 2014

Chemical and physical transformations of organic aerosol from the photo-oxidation of open biomass burning emissions in an environmental chamber, Atmos. Chem. Phys., 11, 7669–7686, doi:10.5194/acp-11-7669-2011, 2011.

Heringa, M. F., DeCarlo, P. F., Chirico, R., Tritscher, T., Dommen, J., Weingartner, E., Richter, R., Wehrle, G., Prévôt, A. S. H., and Baltensperger, U.: Investigations of primary and secondary particulate matter of different wood combustion appliances with a high-resolution time-of-flight aerosol mass spectrometer, Atmos. Chem. Phys., 11, 5945–5957, doi:10.5194/acp-11-5945-2011, 2011.

Hobbs, P. V., Sinha, P., Yokelson, R. J., Christian, T. J., Blake, D. R., Gao, S., Kirchstetter, T. W., Novakov, T., and Pilewskie, P.: Evolution of gases and particles from a savanna fire in South Africa, J. Geophys. Res., 108, 8485, doi:10.1029/2002JD002352, 2003.

Holmes, C. D., Prather, M. J., and Vinken, G. C. M.: The climate impact of ship NO_x emissions: an improved estimate accounting for plume chemistry, Atmos. Chem. Phys., 14, 6801–6812, doi:10.5194/acp-14-6801-2014, 2014.

Huffman, J. A., Jayne, J. T., Drewnick, F., Aiken, A. C., Onasch, T., Worsnop, D. R., and Jimenez, J. L.: Design, modeling, optimization, and experimental tests of a particle beam width probe for the aerodyne aerosol mass spectrometer, Aerosol Sci. Tech., 39, 1143–1163, 2005.

Jacob, D., Wofsy, S., Bakwin, P., Fan, S.-M., Harriss, R., Talbot, R., Bradshaw, J., Sandholm, S., Singh, H., Browell, E. V., Gregory, G., Sachse, G., Shipham, M., Blake, D., and Fitzjarrald, D.: Summertime photochemistry of the troposphere at high northern latitudes, J. Geophys. Res., 97, 16421–16431, 1992.

Jacob, D. J.: Heterogeneous chemistry and tropospheric ozone, Atmos. Environ., 34, 2131–2159, 2000.

Jacobson, M. Z.: Development and application of a new air pollution modeling system – II. Aerosol module structure and design, Atmos. Environ., 31, 131–144, 1997.

Jacobson, M. Z.: Analysis of aerosol interactions with numerical techniques for solving coagulation, nucleation, condensation, dissolution, and reversible chemistry among multiple size distributions, J. Geophys. Res., 107, 4366–4388, doi:10.1029/2001JD002.044, 2002.

Jacobson, M. Z.: Fundamentals of Atmospheric Modeling, 2nd edn., Cambridge University Press, 2005.

Jaffe, D. A. and Wigder, N. L.: Ozone production from wildfires: a critical review, Atmos. Environ., 51, 1–10, doi:10.1016/j.atmosenv.2011.11.063, 2012.

ACPD
14, 32427–32489, 2014

Jaffe, D. A., Wigder, N., Downey, N., Pfister, G., Boynard, A., and Reid, S. B.: Impact of wildfires on ozone exceptional events in the western US, Environ. Sci. Technol., 47, 11065–11072, 2013.

Jenkin, M. E., Saunders, S. M., and Pilling, M. J.: The tropospheric degradation of volatile organic compounds: a protocol for mechanism development, Atmos. Environ., 31, 81–104, doi:10.1016/S1352-2310(96)00105-7, ISSN 1352-2310, 1997.

Jenkin, M. E., Saunders, S. M., Wagner, V., and Pilling, M. J.: Protocol for the development of the Master Chemical Mechanism, MCM v3 (Part B): tropospheric degradation of aromatic volatile organic compounds, Atmos. Chem. Phys., 3, 181–193, doi:10.5194/acp-3-181-2003, 2003.

Jiang, X., Wiedinmyer, C., and Carlton, A. G.: Aerosols from fires: an examination of the effects on ozone photochemistry in the Western United States, Environ. Sci. Technol., 46, 11878–11886, 2012.

Jimenez, J. L., Canagaratna, M. R., Donahue, N. M., Prevot, A. S. H., Zhang, Q., Kroll, J. H., DeCarlo, P. F., Allan, J. D., Coe, H., Ng, N. L., Aiken, A. C., Docherty, K. S., Ulbrich, I. M., Grieshop, A. P., Robinson, A. L., Duplissy, J., Smith, J. D., Wilson, K. R., Lanz, V. A., Hueglin, C., Sun, Y. L., Tian, J., Laaksonen, A., Raatikainen, T., Rautiainen, J, Vaattovaara, P., Ehn, M., Kulmala, M., Tomlinson, J. M., Collins, D. R., Cubison, M. J., Dunlea, E. J., Huffman, J. A., Onasch, T. B., Alfarra, M. R., Williams, P. I., Bower, K., Kondo, Y., Schneider, J., Drewnick, F., Borrmann, S., Weimer, S., Demerjian, K., Salcedo, D., Cottrell, L., Griffin, R., Takami, A., Miyoshi, T., Hatakeyama, S., Shimono, A., Sun, J. Y., Zhang, Y. M., Dzepina, K., Kimmel, J. R., Sueper, D., Jayne, J. T., Herndon, S. C., Trimborn, A. M., Williams, L. R., Wood, E. C., Middlebrook, A. M., Kolb, C. E., Baltensperger, U., and Worsnop, D. R.: Evolution of organic aerosols in the atmosphere, Science, 326, 1525–1529, 2009.

Jost, C., Trentmann, J., Sprung, D., Andreae, M. O., McQuaid, J. B., and Barjat, H.: Trace gas chemistry in a young biomass burning plume over Namibia: observations and model simulations, J. Geophys. Res., 108, 8482–8494, doi:10.1029/2002JD002431, 2003.

Kidd, C., Perraud, V., Wingen, L. M., and Finlayson-Pitts, B. J.: Integrating phase and composition of secondary organic aerosol from the ozonolysis of α-pinene, P. Natl. Acad. Sci. USA, 111, 7552–7557, doi:10.1073/pnas.1322558111, 2014.

ACPD
14, 32427–32489, 2014

Kusik, C. and Meissner, H.: Electrolyte activity coefficients in inorganic processing, in: Fundamental Aspects of Hydrometallurgical Processes, AIChE Symposium Series, edited by: Chapman, T., Taularides, L., Hubred, G., and Wellek, R., AIChE, New York, 14–20, 1978.
Lapina, K., Honrath, R., Owen, R. C., Val Martin, M., and Pfister, G.: Evidence of significant large-scale impacts of boreal fires on ozone levels in the midlatitude Northern Hemisphere free troposphere, Geophys. Res. Lett., 33, L10815, doi:10.1029/2006GL025878, 2006.
Madronich, S. and Flocke, S.: The role of solar radiation in atmospheric chemistry, in: Handbook of Environmental Chemistry, edited by: Boule, P., Springer, 1–26, 1998.
Mason, S. A., Field, R. J., Yokelson, R. J., Kochivar, M. A., Tinsley, M. R., Ward, D. W., and Hao, W. M.: Complex effects arising in smoke plume simulations due to the inclusion of direct emissions of oxygenated organic species from biomass combustion, J. Geophys. Res., 106, 12527–12539, 2001.
Mason, S. A., Trentmann, J., Winterrath, T., Yokelson, R. J., Christian, T. J., Carlson, L. J., Warner, T. R., Wolfe, L. C., and Andreae, M. O.: Intercomparison of two box models of the chemical evolution in biomass-burning smoke plumes, J. Atmos. Chem., 55, 273–297, doi:10.1007/s10874-006-9039-5, 2006.
Mauzerall, D. L., Logan, J. A., Jacob, D. J., Anderson, B. E., Blake, D. R., Bradshaw, J. D., Heikes, B., Sachse, G. W., Singh, H., and Talbot, B.: Photochemistry in biomass burning plumes and implications for tropospheric ozone over the tropical South Atlantic, J. Geophys. Res., 103, 8401–8423, 1998.
Nenes, A., Pandis, S. N., and Pilinis, C.: ISORROPIA: a new thermodynamic equilibrium model for multiphase multicomponent inorganic aerosols, Aquat. Geochem., 4, 123–152, 1998.
Pankow, J. F.: An absorption model of gas/particle partitioning of organic compounds in the atmosphere, Atmos. Environ., 28, 185–188, 1994a.
Pankow, J. F.: An absorption model of the gas/aerosol partitioning involved in the formation of secondary organic aerosol, Atmos. Environ., 28, 189–193, 1994b.
Parrington, M., Palmer, P. I., Lewis, A. C., Lee, J. D., Rickard, A. R., Di Carlo, P., Taylor, J. W., Hopkins, J. R., Punjabi, S., Oram, D. E., Forster, G., Aruffo, E., Moller, S. J., Bauguitte, S. J.-B., Allan, J. D., Coe, H., and Leigh, R. J.: Ozone photochemistry in boreal biomass burning plumes, Atmos. Chem. Phys., 13, 7321–7341, doi:10.5194/acp-13-7321-2013, 2013.
Paulot, F., Crounse, J. D., Kjaergaard, H. G., Kroll, J. H., Seinfeld, J. H., and Wennberg, P. O.: Isoprene photooxidation: new insights into the production of acids and organic nitrates, Atmos. Chem. Phys., 9, 1479–1501, doi:10.5194/acp-9-1479-2009, 2009a.

ACPD
14, 32427–32489, 2014

Paulot, F., Kurten, A., St Clair, J. M., Seinfeld, J. H., and Wennberg, P. O.: Unexpected epoxide formation in the gas-phase photooxidation of isoprene, Science, 325, 730–733, 2009b.
Petters, M. D. and Kreidenweis, S. M.: A single parameter representation of hygroscopic growth and cloud condensation nucleus activity, Atmos. Chem. Phys., 7, 1961–1971, doi:10.5194/acp-7-1961-2007, 2007.
Pfister, G., Emmons, L. K., Hess, P. G., Honrath, R., Lamarque, J. F., Val Martin, M., Owen, R. C., Avery, M. A., Browell, E. V., Holloway, J. S., Nedelec, P., Purvis, R., Ryerson, R. B., Sachse, G. W., and Schlager, H.: Ozone production from the 2004 North American boreal fires, J. Geophys. Res., 111, D24S07, doi:10.1029/2006JD007695, 2006.
Pun, B. K., Griffin, R. J., Seigneur, C., and Seinfeld, J. H.: Secondary organic aerosol, 2. Thermodynamic model for gas/particle partitioning of molecular constituents, J. Geophys. Res., 107, 4333–4347, doi:10.1029/2001JD000542, 2002.
Radke, L. F., Hegg, D. A., Hobbs, P. V., Nance, J. D., Lyons, J. H., Laursen, K. K., Weiss, R. E., Riggan, P. J., and Ward, D. E.: Particulate and Trace Gas Emissions from Large Biomass Fires in North America, Global Biomass Burning – Atmospheric, Climatic, and Biospheric Implications, MIT Press, Cambridge, MA, 209–224, 1991.
Reid, J. S. and Hobbs, P. V.: Physical and optical properties of young smoke from individual biomass fires in Brazil, J. Geophys. Res., 103, 32013–32030, 1998.
Reid, J. S., Eck, T. F., Christopher, S. A., Koppmann, R., Dubovik, O., Eleuterio, D. P., Holben, B. N., Reid, E. A., and Zhang, J.: A review of biomass burning emissions part III: intensive optical properties of biomass burning particles, Atmos. Chem. Phys., 5, 827–849, doi:10.5194/acp-5-827-2005, 2005a.
Reid, J. S., Koppmann, R., Eck, T. F., and Eleuterio, D. P.: A review of biomass burning emissions part II: intensive physical properties of biomass burning particles, Atmos. Chem. Phys., 5, 799–825, doi:10.5194/acp-5-799-2005, 2005b.
Resch, T.: A framework for modeling suspended multicomponent particulate systems with applications to atmospheric aerosols, Ph.D. thesis, Massachusetts Institute of Technology, 1995.
Robinson, A. L., Donahue, N. M., Shrivastava, M. K., Weitkamp, E. A., Sage, A. M., Grieshop, A. P., Lane, T. E., Pierce, J. R., and Pandis, S. N.: Rethinking organic aerosols: semivolatile emissions and photochemical aging, Science, 315, 1259–1262, 2007.
Sander, S. P., Abbatt, J., Barker, J. R., Burkholder, J. B., Friedl, R. R., Golden, D. M., Huie, R. E., Kolb, C. E., Kurylo, M. J., Moortgat, G. K., Orkin, V. L., and Wine, P. H.: Chemical Kinetics and

ACPD
14, 32427–32489, 2014

Photochemical Data for Use in Atmospheric Studies, Evaluation No. 17, JPL Publication 10-6, Jet Propulsion Laboratory, Pasadena, available at: http://jpldataeval.jpl.nasa.gov, 2011.

Saunders, S. M., Jenkin, M. E., Derwent, R. G., and Pilling, M. J.: Protocol for the development of the Master Chemical Mechanism, MCM v3 (Part A): tropospheric degradation of non-aromatic volatile organic compounds, Atmos. Chem. Phys., 3, 161–180, doi:10.5194/acp-3-161-2003, 2003.

Seinfeld, J. H. and Pandis, S. N.: Atmospheric Chemistry and Physics, John Wiley and Sons, New York, NY, 1998.

Singh, H. B., Cai, C., Kaduwela, A., Weinheimer, A., and Wisthaler, A.: Interactions of fire emissions and urban pollution over California: ozone formation and air quality simulations, Atmos. Environ., 56, 45–51, 2012.

Sommers, W. T., Loehman, R. A., and Hardy, C. C.: Wildland fire emissions, carbon, and climate: science overview and knowledge needs, For. Ecol. Manage., 317, 1–8, doi:10.1016/j.foreco.2013.12.014, available at: http://www.treesearch.fs.fed.us/pubs/45726, 2014.

Steele, H. D.: Investigations of cloud altering effects of atmospheric aerosols using a new mixed eulerian-lagrangian aerosol model, Ph.D. thesis, Massachusetts Institute of Technology, available at: http://web.mit.edu/cgcs/www/MIT_CGCS_Rpt74.pdf, 2004.

Stemmler, K., Ammann, M., Donders, C., Kleffmann, J., and George, C.: Photosensitized reduction of nitrogen dioxide on humic acid as a source of nitrous acid, Nature, 440, 195–198, doi:10.1038/nature04603, 2006.

Stemmler, K., Ndour, M., Elshorbany, Y., Kleffmann, J., D'Anna, B., George, C., Bohn, B., and Ammann, M.: Light induced conversion of nitrogen dioxide into nitrous acid on submicron humic acid aerosol, Atmos. Chem. Phys., 7, 4237–4248, doi:10.5194/acp-7-4237-2007, 2007.

Stokes, R. H. and Robinson, R. A.: Interactions in aqueous nonelectrolyte solutions. I. Solute-solvent equilibria, J. Phys. Chem., 70, 2126–2130, 1966.

Sudo, K. and Akimoto. H.: Global source attribution of tropospheric ozone: long-range transport from various source regions, J. Geophys. Res., 112, D12302, doi:10.1029/2006JD007992, 2007.

Trentmann, J., Andreae, M. O., and Graf, H.-F.: Chemical processes in a young biomass-burning plume, J. Geophys. Res., 108, 4705–4714, doi:10.1029/2003JD003732, 2003.

ACPD
14, 32427–32489, 2014

Trentmann, J., Yokelson, R. J., Hobbs, P. V., Winterrath, T., Christian, T. J., Andreae, M. O., and Mason, S. A.: An analysis of the chemical processes in the smoke plume from a savannah fire, J. Geophys. Res., 110, D12301, doi:10.1029/2004JD005628, 2005.

Vakkari, V., Kerminen, V., Beukes, J.P., Tiitta, P., van Zyl, P. G., Josipovic, M., Venter, A. D., Jaars, K., Worsnop, D. R., Kulmala, M., and Laakso, L.: Rapid changes in biomass burning aerosols by atmospheric oxidation, Geophys. Res. Lett., 41, 2644–2651, doi:10.1002/2014GL059396, 2014.

Val Martin, M., Honrath, R. E., Owen, R. C., Pfister, G., Fialho, P., and Barata, F.: Significant enhancements of nitrogen oxides, ozone and aerosol black carbon in the North Atlantic lower free troposphere resulting from North American boreal wildfires, J. Geophys. Res., 111, D23S60, doi:10.1029/2006JD007530, 2006.

van der Werf, G. R., Randerson, J. T., Giglio, L., Collatz, G. J., Mu, M., Kasibhatla, P. S., Morton, D. C., DeFries, R. S., Jin, Y., and van Leeuwen, T. T.: Global fire emissions and the contribution of deforestation, savanna, forest, agricultural, and peat fires (1997–2009), Atmos. Chem. Phys., 10, 11707–11735, doi:10.5194/acp-10-11707-2010, 2010.

Vinken, G. C. M., Boersma, K. F., Jacob, D. J., and Meijer, E. W.: Accounting for non-linear chemistry of ship plumes in the GEOS-Chem global chemistry transport model, Atmos. Chem. Phys., 11, 11707–11722, doi:10.5194/acp-11-11707-2011, 2011.

Warneke, C., Roberts, J. M., Veres, P., Gilman, J., Kuster, W. C., Burling, I., Yokelson, R. J., and de Gouw, J. A.: VOC identification and inter-comparison from laboratory biomass burning using PTR-MS and PIT-MS, Int. J. Mass Spectrom. Ion Proc., 303, 6–14, doi:10.1016/j.ijms.2010.12.002, 2011.

Wilson, J. C., Lafleur, B. G., Hilbert, H., Seebaugh, W. R., Fox, J., Gesler, D. W., Brock, C. A., Huebert, B. J., and Mullen, J.: Function and performance of a low turbulence inlet for sampling supermicron particles from aircraft platforms, Aerosol Sci. Tech., 38, 790–802, 2004.

Yarwood, G., Rao, S., Yocke, M., and Whitten, G. Z.: Updates to the carbon bond chemical mechanism: CB05, RT-04-00675, Prepared for Deborah Luecken, US Environmental Protection Agency Research Triangle Park, NC 27703, ENVIRON, available at: http://www.camx.com/publ/pdfs/cb05_final_report_120805.pdf, 2005.

Yokelson, R. J., Goode, J. G., Ward, D. E., Susott, R. A., Babbitt, R. E., Wade, D. D., Bertschi, I., Griffith, D. W. T., and Hao, W. M.: Emissions of formaldehyde, acetic acid, methanol, and other trace gases from biomass fires in North Carolina measured by

ACPD
14, 32427–32489, 2014

airborne Fourier transform infrared spectroscopy, J. Geophys. Res., 104, 30109–30126, doi:10.1029/1999JD900817, 1999.
Yokelson, R. J., Bertschi, I. T., Christian, T. J., Hobbs, P. V., Ward, D. E., and Hao, W. M.: Trace gas measurements in nascent, aged, and cloud-processed smoke from African savanna fires by airborne fourier transform infrared spectroscopy (AFTIR), J. Geophys. Res., 108, 8478–8491, doi:10.1029/2002JD002322, 2003.
Yokelson, R. J., Urbanski, S. P., Atlas, E. L., Toohey, D. W., Alvarado, E. C., Crounse, J. D., Wennberg, P. O., Fisher, M. E., Wold, C. E., Campos, T. L., Adachi, K., Buseck, P. R., and Hao, W. M.: Emissions from forest fires near Mexico City, Atmos. Chem. Phys., 7, 5569–5584, doi:10.5194/acp-7-5569-2007, 2007.
Yokelson, R. J., Crounse, J. D., DeCarlo, P. F., Karl, T., Urbanski, S., Atlas, E., Campos, T., Shinozuka, Y., Kapustin, V., Clarke, A. D., Weinheimer, A., Knapp, D. J., Montzka, D. D., Holloway, J., Weibring, P., Flocke, F., Zheng, W., Toohey, D., Wennberg, P. O., Wiedinmyer, C., Mauldin, L., Fried, A., Richter, D., Walega, J., Jimenez, J. L., Adachi, K., Buseck, P. R., Hall, S. R., and Shetter, R.: Emissions from biomass burning in the Yucatan, Atmos. Chem. Phys., 9, 5785–5812, doi:10.5194/acp-9-5785-2009, 2009.
Zaveri, R. A., Easter, R. C., Shilling, J. E., and Seinfeld, J. H.: Modeling kinetic partitioning of secondary organic aerosol and size distribution dynamics: representing effects of volatility, phase state, and particle-phase reaction, Atmos. Chem. Phys., 14, 5153–5181, doi:10.5194/acp-14-5153-2014, 2014.
Zdanovskii, A. B.: New methods for calculating solubilities of electrolytes in multi-component systems, Zh. Fiz. Kim., 22, 1475–1485, 1948.
Zhang, L., Jacob, D. J., Yue, X., Downey, N. V., Wood, D. A., and Blewitt, D.: Sources contributing to background surface ozone in the US Intermountain West, Atmos. Chem. Phys., 14, 5295–5309, doi:10.5194/acp-14-5295-2014, 2014.

ACPD
14, 32427–32489, 2014

Table 1. Initial temperatures (T, in K) and mixing ratios (ppbv) used for the EPA chamber simulations. Note HONO initial concentration is set at 0.05 ppbv for all runs. PRO = propene, t-BUT = trans-2-butene, BUT = n-butane, OCT = octane, TOL = toluene, and XYL = m-xylene.

Case	T	NO	NO_2	CO	HCHO	C_2H_4	PRO	t-BUT	BUT	OCT	TOL	XYL
96A	303.9	64.13	45.14	0	21.73	12.29	9.907	7.779	62.03	16.15	15.96	15.13
96B	303.9	64.25	46.83	0	21.66	12.29	9.907	7.779	62.03	16.15	15.96	15.13
97A	303.7	3.107	2.175	0	12.2	8.386	7.605	6.649	52	11.16	10.59	9.833
97B	303.7	3.168	2.039	0	12.05	8.208	7.566	6.513	52	11.28	10.65	10.08
80A	303.6	62.54	29.69	0	112.3	76.64	61.63	58.43	365.7	96.88	90.98	86.35
80B	303.6	62.54	29.69	0	112.3	76.64	61.63	58.43	365.7	96.88	90.98	86.35
81A	303.5	33.47	16.43	0	59.27	41.41	31.91	29.46	187.1	60.08	50.47	46.97
81B	303.5	33.5	16.51	0	59.01	41.42	32.23	29.31	185.7	60.08	49.91	46.7
128A	302.6	30.59	17.03	0	10.98	8.751	8.258	7.124	53.93	12.17	11.67	11.57
83A	303.5	31.69	16.17	20.67	18.32	26.02	14.68	12.97	88.29	24	20.23	19.19
84B	303.5	33.61	17.51	20.67	24.72	16.34	16.79	15.32	100.4	29	24.23	22.94
110B	303.4	19.57	11.91	20.67	0	9.763	8.834	7.81	58.71	12.99	12.43	12.7
114A	302.7	19.88	10.9	20.67	21	8.219	7.473	6.664	50.45	12.67	11.9	11.51
127B	302.8	18.65	10.37	20.67	11.82	8.636	8.025	6.791	52.78	11.88	11.33	11.18
137A	303.4	18.29	10.28	20.67	11.01	8.845	8.476	7.335	55.43	12.17	11.35	13.29
143A	303.5	18.41	10.26	20.67	0.1523	8.688	8.126	6.791	51.84	11.48	10.95	10.84
143B	303.5	18.5	10.3	20.67	0	8.782	8.134	7.053	52.82	11.89	11.39	11.21
151B	303.7	18.23	11.39	20.67	10.12	8.292	7.683	6.77	50.22	12.66	11.57	11.95
163B	303.9	14.87	8.699	20.67	10.79	7.781	7.341	6.468	48.11	11.94	11.51	11.29
167A	304.1	18.02	11.05	20.67	10.87	8.48	8.111	7.113	52.25	12.31	11.57	11.64
168B	303.9	18.16	10.83	20.67	10.87	8.677	8.168	6.921	51.06	12.09	11.26	11.62
226A	304.7	19.56	11.3	45.65	0	9.064	8.274	8.5	47.09	13.15	12.89	12.73
226B	304.7	19.5	11.37	41.32	0	9.22	8.481	8.849	47.81	13.46	13.05	13.37
229B	303.3	20.18	11.62	41.32	0	10.26	9.799	9.776	56.15	15.27	14.1	15.51
230A	302.6	20.68	12.53	41.32	0	9.08	8.81	9.089	50.51	14.29	13.25	14
100A	303.6	3.07	2.254	41.32	9.2	5.34	4.65	3.885	35	6.899	5.851	5.581
180B	304.8	31.64	19.92	41.32	33	34.38	32.62	34.36	186.6	51.03	48.85	47.51
181B	305.1	13.17	10.8	41.32	32	35.49	32.88	34.78	188.1	47.84	45.71	44.52
182B	304.6	30.15	22.52	41.32	15	18.16	16.85	17.89	98.27	23.83	22.59	22.21
188B	304.4	7.546	6.216	41.32	8	8.663	8.183	8.404	49.4	11.87	11.27	11.07
189B	302.0	7.754	5.641	41.32	16.5	16.94	15.63	16.35	91.4	21.89	20.93	20.17
190B	304.4	63.32	34.07	41.32	10.5	8.578	7.998	8.121	49.63	12.94	12.43	12
191B	301.8	8.104	4.7	41.32	4	4.211	4.15	4.184	27.14	6.464	6.162	6.154
192B	304.0	3.916	3.08	41.32	6	8.259	7.881	8.252	48.32	10.46	9.853	9.844
193B	304.4	32	15.67	41.32	4	4.619	4.461	4.337	28.08	6.068	5.762	5.749
197B	304.9	64.16	39.59	41.32	43	34.03	31.52	33.29	183	44.37	42.29	41.4
113A	303.1	44.42	24.84	41.32	0	16.32	14.88	12.91	91.75	24	22.9	22.59
180A	304.8	31.61	20.22	41.32	33	34.38	32.62	34.36	186.6	51.03	48.85	47.51

ACPD
14, 32427–32489, 2014

Table 2. Off-gassing, wall reaction, and selected photolysis rates used for the EPA chamber simulations.

Reaction	Rate (s^{-1})
OffGas → HONO	5.5424×10^{-8} (Chamber A)
OffGas → HONO	3.6805×10^{-8} (Chamber B)
OffGas → HCHO	8.33×10^{-8}
O_3 → Wall O_3	1.8×10^{-6}
NO_2 → 0.2 HONO + 0.8 Wall NO_X	2.67×10^{-6}
N_2O_5 → Wall NO_X	4.67×10^{-5}
NO_2 → NO + O	4.333×10^{-3}
$O_3 \rightarrow O^{1-D} + O_2$	2.947×10^{-6}
$O_3 \rightarrow O + O_2$	8.6667×10^{-4}
HONO → 0.9 OH + 0.9 NO + 0.1 HO_2 + 0.1 NO_2	8.6667×10^{-4}
$NO_3 \rightarrow NO + O_2$	8.233×10^{-3}
HCHO → HO_2 + HO_2 + CO	4.767×10^{-6}
Acetaldehyde → CH_3O_2 + HO_2 + CO	$5{,}776 \times 10^{-7}$
Acetone → CH_3CO_3 + CH_3O_2	4.767×10^{-8}
MGLY → CH_3CO_3 + CO + HO_2	6.5×10^{-5}

ACPD
14, 32427–32489, 2014

Table 3. Initial and background trace gas concentrations for the ASP simulations of the Williams Fire smoke plume. Only compounds with non-zero values are listed. "GEOS-Chem" refers to the GEOS-Chem model output from the study of Fischer et al. (2014).

Species	Initial Conc. (ppbv)	Background Conc. (ppbv)	Initial Conc. Source	Background Conc. Source
CO	1.00E+04	1.29E+02	Akagi et al. (2012)	–
CO_2	5.28E+05	3.90E+05	Akagi et al. (2012)	Approximate
Trace	1.00E+03	0.00E+00	–	–
NO	1.14E+02	1.50E−02	Akagi et al. (2012)	GEOS-Chem
NO_2	2.27E+02	3.90E−02	Akagi et al. (2012)	GEOS-Chem
O_3	0.00E+00	5.00E+01	Akagi et al. (2012)	Akagi et al. (2012)
H_2O_2	7.55E−01	7.55E−01	–	GEOS-Chem
HONO	3.95E+01	0.00E+00	Akagi et al. (2012)	–
SO_2	3.79E+01	1.20E−01	Akagi et al. (2011) (chaparral)	GEOS-Chem
HNO_3	4.10E−01	4.10E−01	–	GEOS-Chem
H_2SO_4	1.00E−04	0.00E+00	–	–
HCl	1.95E+01	1.00E−05	Akagi et al. (2011) (chaparral)	–
NH_3	3.79E+02	9.60E−04	Akagi et al. (2012)	GEOS-Chem
H_2	3.74E+03	1.00E−05	Akagi et al. (2011) (savannah)	–
			C_1 Parent Compounds	
CH_4	2.76E+03	1.90E+03	Akagi et al. (2012)	Approximate
HCHO	1.63E+02	3.30E−01	Akagi et al. (2012)	GEOS-Chem
Methanol	1.65E+02	0.00E+00	Akagi et al. (2012)	–
Formic Acid	6.50E+00	0.00E+00	Akagi et al. (2012)	–
HCN	1.28E+02	0.00E+00	Akagi et al. (2012)	–
			C_2 Parent Compounds	
Ethylene	1.26E+02	0.00E+00	Akagi et al. (2012)	–
Ethane	5.28E+01	0.00E+00	Akagi et al. (2011) (chaparral)	–
Acetaldehyde	5.70E+01	0.00E+00	Akagi et al. (2011) (savannah)	–
Ethanol	9.87E−01	0.00E+00	Andreae and Merlet (2001) with 2009 updates (savannah)	–
Acetic Acid	1.39E+02	0.00E+00	Akagi et al. (2012)	–
Glyoxal	8.52E+01	0.00E+00	Andreae and Merlet (2001) with 2009 updates (savannah)	–
Acetylene	2.68E+01	0.00E+00	Akagi et al. (2012)	
			C_3 Parent Compounds	
Propene	4.74E+01	0.00E+00	Akagi et al. (2012)	–
Propane	1.78E+01	0.00E+00	Akagi et al. (2011) (chaparral)	–
Acrolein	5.92E+00	0.00E+00	Andreae and Merlet (2001) with 2009 updates (savannah)	–
Propanal	6.42E−01	0.00E+00	Andreae and Merlet (2001) with 2009 updates (savannah)	–
Acetone	1.21E+01	0.00E+00	Akagi et al. (2011) (savannah)	–
n-Propanol	1.84E+00	0.00E+00	Andreae and Merlet (2001) with 2009 updates (savannah)	–
Methyl Glyoxal	4.47E+01	0.00E+00	Andreae and Merlet (2001) with 2009 updates (savannah)	–

ACPD
14, 32427–32489, 2014

Table 3. Continued.

Species	Initial Conc. (ppbv)	Background Conc. (ppbv)	Initial Conc. Source	Background Conc. Source
			C_4 Parent Compounds	
Butadiene	4.23E+00	0.00E+00	Akagi et al. (2011) (savannah)	–
1-Butene	3.34E+00	0.00E+00	Akagi et al. (2011) (savannah)	–
cis-2-Butene	6.80E−01	0.00E+00	Akagi et al. (2011) (savannah)	–
trans-2-Butene	8.55E−01	0.00E+00	Akagi et al. (2011) (savannah)	–
i-Butene	1.89E+00	0.00E+00	Akagi et al. (2011) (savannah)	–
n-Butane	9.87E+00	0.00E+00	Akagi et al. (2011) (chaparral)	–
i-Butane	3.23E−01	0.00E+00	Akagi et al. (2011) (savannah)	–
Butanal	3.34E+00	0.00E+00	Andreae and Merlet (2001) with 2009 updates (savannah)	–
MEK	1.53E+01	0.00E+00	Andreae and Merlet (2001) with 2009 updates (savannah)	–
n-Butanol	5.00E−01	0.00E+00	Andreae and Merlet (2001) with 2009 updates (savannah)	–
			Lumped Parent Compounds	
FURAN	2.02E+01	0.00E+00	Akagi et al. (2012)	–
ISOP	2.53E+00	0.00E+00	Akagi et al. (2011) (savannah)	–
ALD	7.22E−01	2.00E−02	Andreae and Merlet (2001) with 2009 updates (savannah)	GEOS-Chem
API	3.26E+01	0.00E+00	Akagi et al. (2013)	–
BALD	1.25E+00	0.00E+00	Andreae and Merlet (2001) with 2009 updates (savannah)	–
BEN	1.11E+01	0.00E+00	Akagi et al. (2011) (savannah)	
DIEN	1.20E+00	0.00E+00	Andreae and Merlet (2001) with 2009 updates (savannah)	
HC_5	2.38E+00	1.08E+00	Akagi et al. (2011) (savannah)	GEOS-Chem
KET	1.58E+00	0.00E+00	Andreae and Merlet (2001) with 2009 updates (savannah)	
LIM	3.26E+01	0.00E+00	Akagi et al. (2013)	–
OLI	2.14E+00	0.00E+00	Akagi et al. (2011) (savannah)	
OLT	8.75E−01	0.00E+00	Akagi et al. (2011) (savannah)	
PHEN	1.46E+01	0.00E+00	Akagi et al. (2012)	–
ROH	1.70E+00	0.00E+00	Andreae and Merlet (2001) with 2009 updates (savannah)	
TOL	4.07E+00	0.00E+00	Akagi et al. (2011) (savannah)	
XYM	3.15E−01	0.00E+00	Akagi et al. (2011) (savannah)	
XYP	8.59E−02	0.00E+00	Akagi et al. (2011) (savannah)	
XYO	1.62E−01	0.00E+00	Akagi et al. (2011) (savannah)	
			Highly oxygenated VOCs	
$HOCH_2CHO$	1.85E−01	0.00E+00	Akagi et al. (2012)	–
ACETOL	2.68E+01	0.00E+00	Akagi et al. (2011) (savannah)	–
BIACET	2.79E+01	0.00E+00	Andreae and Merlet (2001) with 2009 updates (savannah)	–
			Organic Nitrates	
PAN	6.61E+00	3.00E−02	Akagi et al. (2012)	GEOS-Chem
PPN	3.20E−03	3.20E−03	GEOS-Chem	GEOS-Chem
CH_3NO_3	2.91E−02	0.00E+00	Akagi et al. (2011) (savannah)	–
			VBS compounds	
$SVOC_3$	2.15E−02	0.00E+00	Grieshop et al. (2009a, b)	–
$SVOC_4$	2.55E−01	0.00E+00	Grieshop et al. (2009a, b)	–
$SVOC_5$	3.08E+00	0.00E+00	Grieshop et al. (2009a, b)	–
$SVOC_6$	3.78E+01	0.00E+00	Grieshop et al. (2009a, b)	–
$SVOC_7$	4.67E+02	0.00E+00	Grieshop et al. (2009a, b)	–

ACPD
14, 32427–32489, 2014

Table 4. Initial and background aerosol mass concentrations for the ASP simulations of the Williams Fire smoke plume. Only compounds with non-zero values are listed. Bold is used for compounds that are components of modeled OA.

Species	Initial Conc. ($\mu g\,m^3$)[a]	Background Conc. ($\mu g\,m^3$)[a]	Initial Conc. Source	Background Conc. Source
OA	849	1.335	Akagi et al. (2012)	GEOS-Chem
$SVOC_3$	**84.9**	–	**Grieshop et al. (2009a, b)**	–
$SVOC_4$	**118.9**	–	**Grieshop et al. (2009a, b)**	–
$SVOC_5$	**280.2**	–	**Grieshop et al. (2009a, b)**	–
$SVOC_6$	**280.2**	–	**Grieshop et al. (2009a, b)**	–
$SVOC_7$	**84.9**	–	**Grieshop et al. (2009a, b)**	–
CPD3[b]	–	**1.335**	–	**GEOS-Chem**
BC	187	0.357	Akagi et al. (2012)	GEOS-Chem
K	1.86	–	Amount needed to neutralize anions	–
NH_4	14.3	1.291	Akagi et al. (2012)	GEOS-Chem
SO_4	0.855	6.603	Akagi et al. (2012)	GEOS-Chem
NO_3	30.4	0.174	Akagi et al. (2012)	GEOS-Chem
Cl	11.9	–	Akagi et al. (2012)	–

[a] Values at the temperature and pressure of the plume (T = 288.4 K, P = 880 hPa).
[b] Extremely low volatility humic-like species, see Alvarado (2008).

ACPD
14, 32427–32489, 2014

Table 5. SVOC chemistry parameters in the mechanisms studied here. See Reactions (R3) and (R4) for definitions of the parameters.

Mechanism	$k_{OH} \times 10^{11}$ (cm^3 $molecule^{-1}$ s^{-1})	μ	n	α	χ	β	δ
Grieshop et al. (2009)	2.0	1.4	2	0	0	0	0
Robinson et al. (2007)	4.0	1.075	1	0	0	0	0
Ahmadov et al. (2012)	1.0	1.075	1	0	0	0	0
Half Fragmentation	1.0	1.075	1	0.5	0	0	0
Optimized SVOC Chemistry	1.0	1.075	1	0.5	1	0.5	0.6

ACPD
14, 32427–32489, 2014

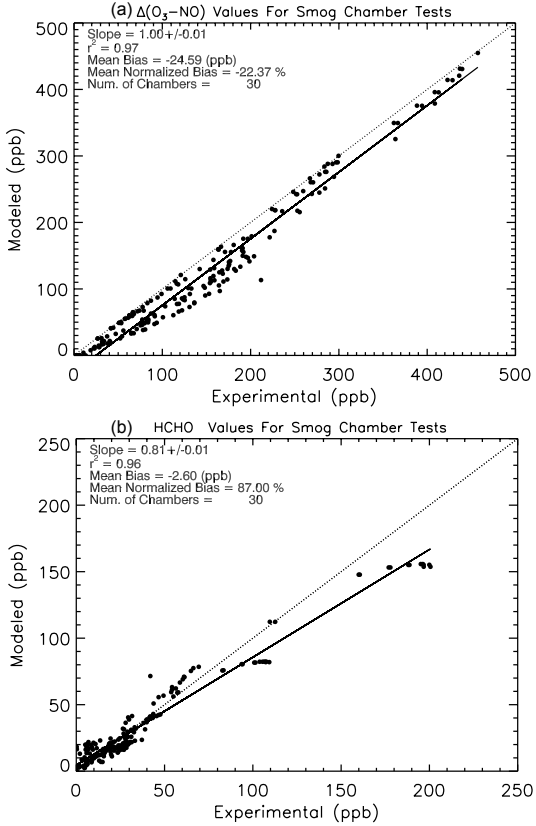

Figure 1. (a) ASP calculated hourly values of $\Delta([O_3] - [NO]) \equiv ([O_3]_{final} - [NO]_{final})/([O_3]_{initial} - [NO]_{initial})$ vs. the values measured in the EPA chamber of Carter et al. (2005) for 30 "full surrogate" experiments. Note that all time points for the 30 chamber experiments are plotted, not just the final values. **(b)** ASP calculated vs. measured formaldehyde (HCHO) values for the chamber experiments.

ACPD
14, 32427–32489, 2014

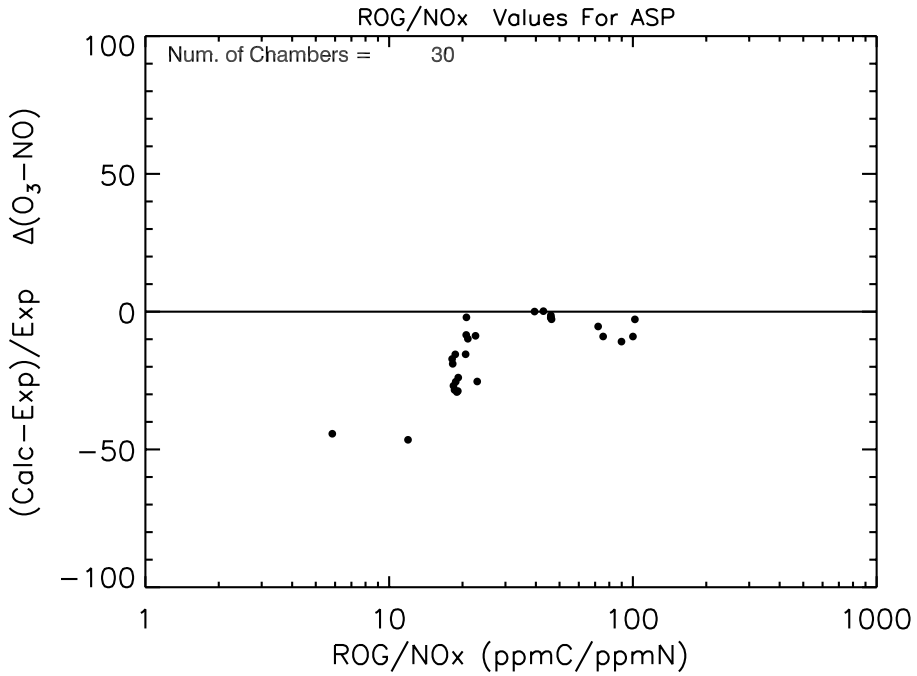

Figure 2. Percentage bias in final $\Delta([O_3] - [NO])$ vs. the initial ratio of reactive organic gases (ROG) to NO_x (ppm C/ppm N) for the chamber experiments.

ACPD
14, 32427–32489, 2014

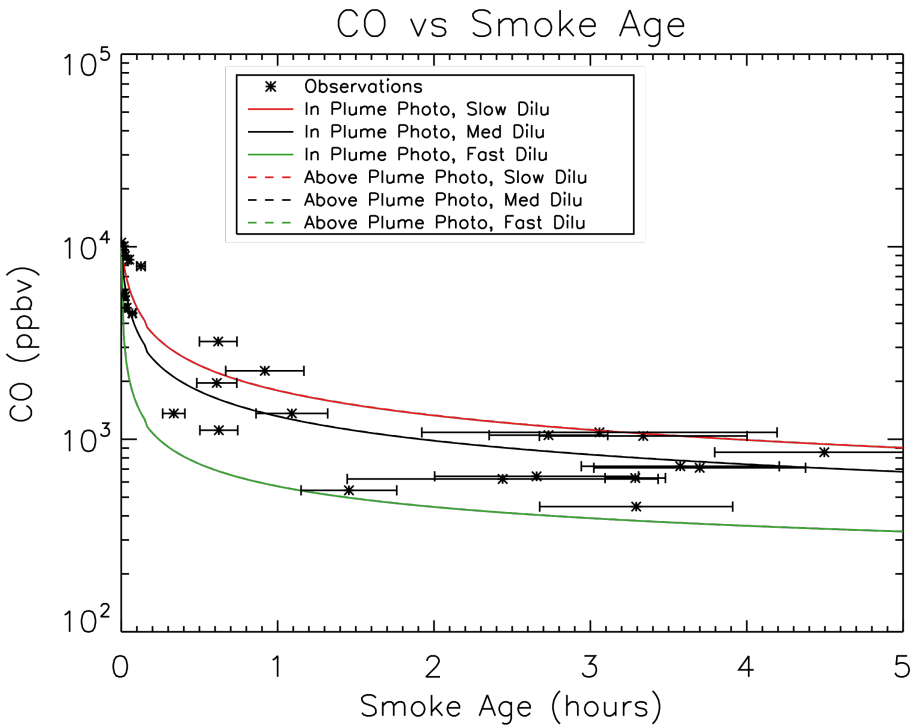

Figure 3. CO mixing ratio (ppbv) vs. smoke age. Red, black, and green are for the slow, best-fit (medium), and fast plume dilution rates. Asterisks are the measured mixing ratios, with the horizontal error bars showing the uncertainty in the estimated age, which is much larger than the uncertainty in the CO mixing ratio.

ACPD
14, 32427–32489, 2014

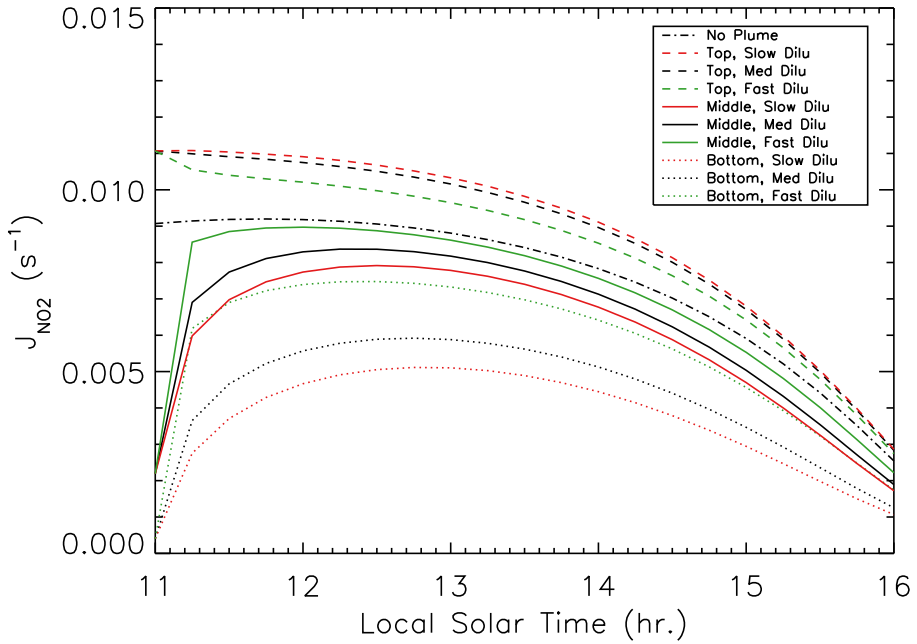

Figure 4. NO_2 photolysis rates (s^{-1}) vs. local time. Red, black, and green are for the slow, best-fit (medium), and fast plume dilution rates. Dashed lines are for photolysis rates above the plume, solid lines are for the middle of the plume, and dotted lines are for the bottom of the plume, as described in the text. The black dot-dashed line is the clear-sky (no plume) photolysis rate.

ACPD
14, 32427–32489, 2014

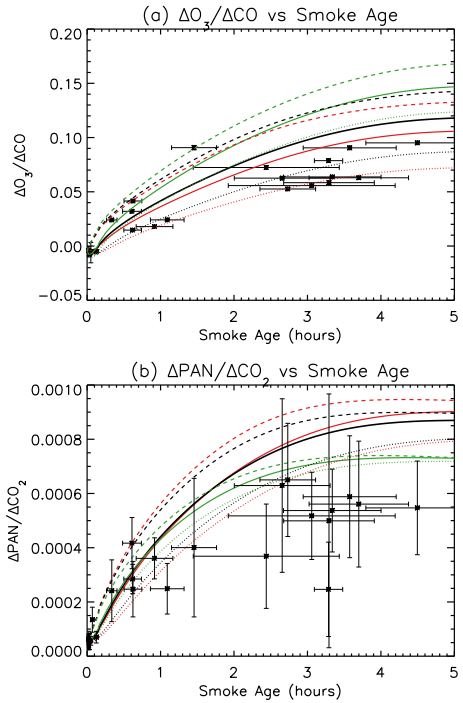

Figure 5. Enhancement ratios (mol mol^{-1}) of **(a)** O_3 to CO and **(b)** PAN to CO_2 vs. estimated smoke age when the chemistry of the unidentified SVOCs is not included in the model. Asterisks are the measured mixing ratios, with the horizontal error bars showing the uncertainty in the estimated age and the vertical error bars showing the uncertainty in the measurement. Red, black, and green are ASP results for the slow, best-fit (medium), and fast plume dilution rates. Dashed lines are for above-plume photolysis rates, while solid lines are for the middle of the plume, and dotted lines are for the bottom of the plume (see the legend in Fig. 4).

ACPD
14, 32427–32489, 2014

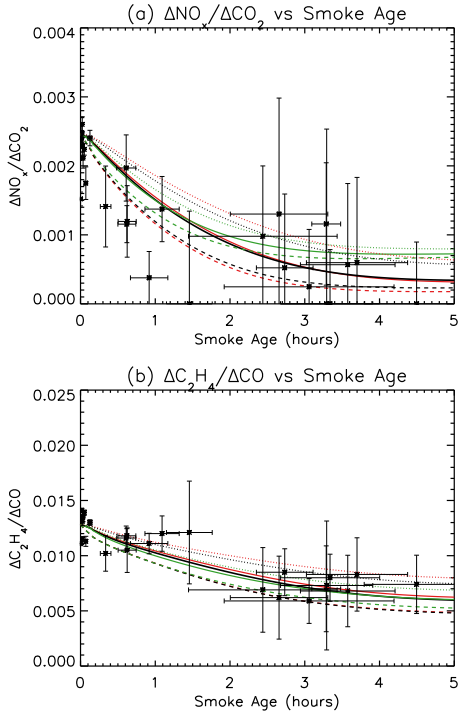

Figure 6. (a) NO_x enhancement ratio (EnR, mol mol^{-1}) to CO_2 vs. estimated smoke age when the chemistry of the unidentified SVOCs is not included in the model. **(b)** EnR of C_2H_4 to CO vs. estimated smoke age. Asterisks are the measured mixing ratios, with the horizontal error bars showing the uncertainty in the estimated age and the vertical error bars showing the uncertainty in the measurement. Red, black, and green are ASP results for the slow, best-fit (medium), and fast plume dilution rates. Dashed lines are for above-plume photolysis rates, while solid lines are for the middle of the plume, and dotted lines are for the bottom of the plume (see the legend in Fig. 4).

ACPD
14, 32427–32489, 2014

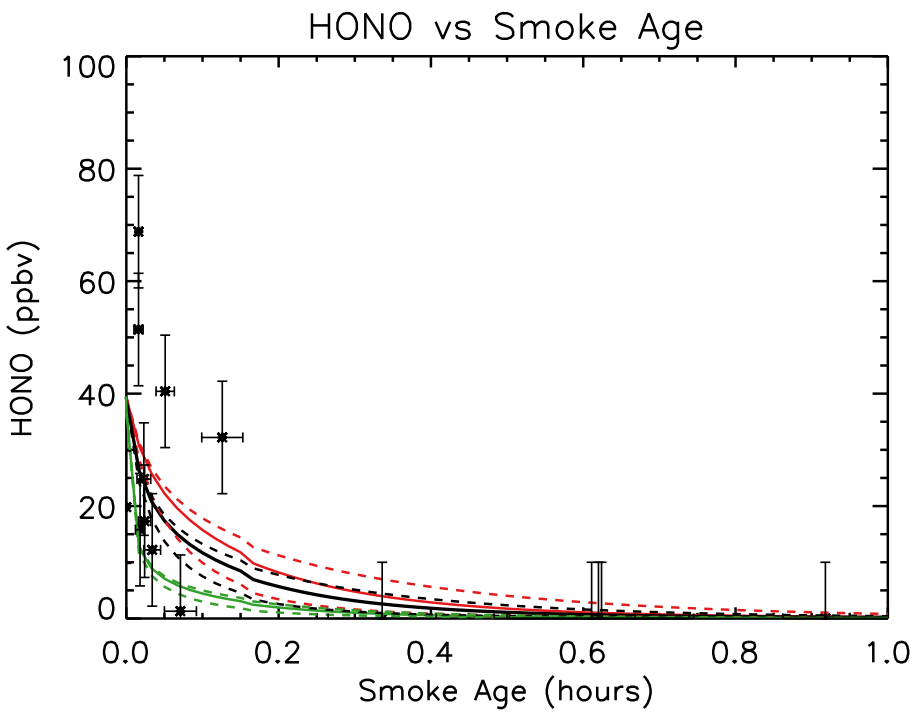

Figure 7. HONO mixing ratio (ppbv) vs. estimated smoke age for the first hour after emission (note difference in *x* axis scale from Figs. 4–6) when the chemistry of the unidentified SVOCs and a downwind HONO source is not included in the model. Asterisks are the measured mixing ratios, with the horizontal error bars showing the uncertainty in the estimated age and the vertical error bars showing the uncertainty in the measurement. Red, black, and green are ASP results for the slow, best-fit (medium), and fast plume dilution rates. Dashed lines are for above-plume photolysis rates, while solid lines are for the middle of the plume, and dotted lines are for the bottom of the plume (see the legend in Fig. 4).

ACPD
14, 32427–32489, 2014

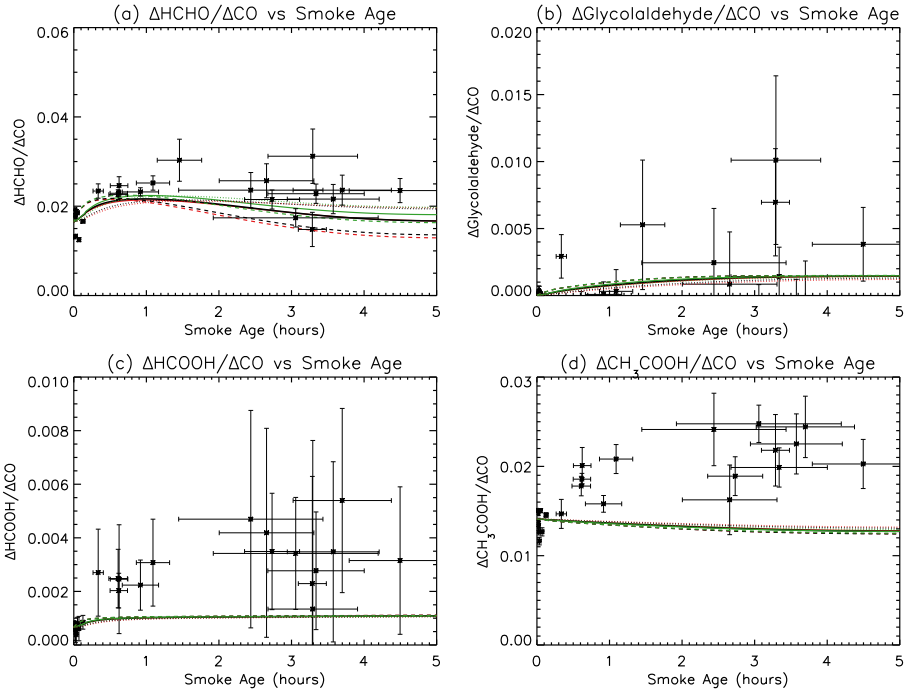

Figure 8. Enhancement ratio (EnR, mol mol^{-1}) of **(a)** HCHO, **(b)** glycoaldehyde ($HCOCH_2OH$), **(c)** formic acid (HCOOH), and **(d)** acetic acid (CH_3COOH) to CO vs. estimated smoke age when the chemistry of the unidentified SVOCs is not included in the model. Asterisks are the measured mixing ratios, with the horizontal error bars showing the uncertainty in the estimated age and the vertical error bars showing the uncertainty in the measurement. Red, black, and green are ASP results for the slow, best-fit (medium), and fast plume dilution rates. Dashed lines are for above-plume photolysis rates, while solid lines are for the in-plume rates, as described in the text.

ACPD
14, 32427–32489, 2014

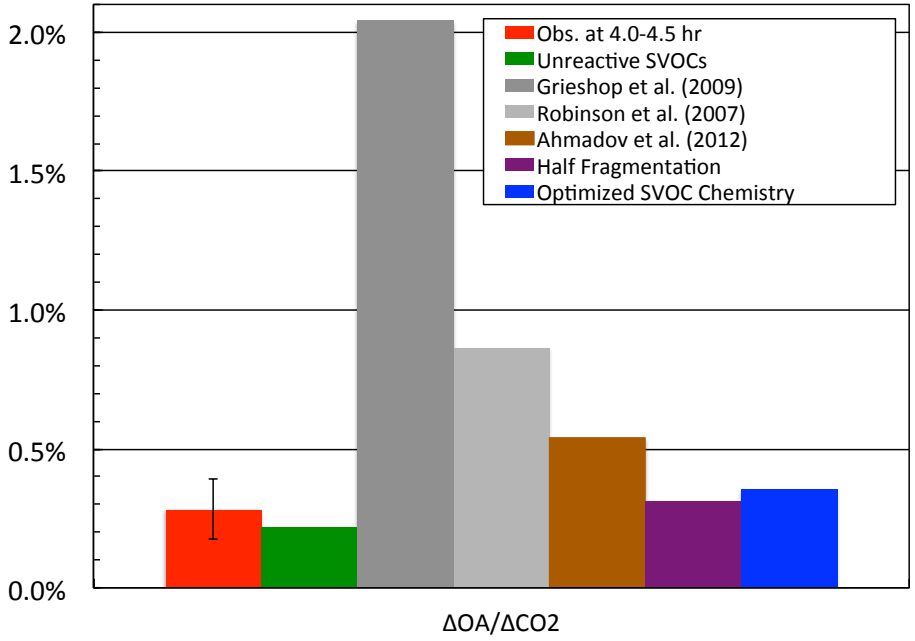

Figure 9. Enhancement ratio (EnR, g g^{-1}) of organic aerosol (OA) to CO_2 after 4 to 4.5 h of smoke aging. The error bars on the observed values are based on the 36 % uncertainty in the AMS observations of OA. All model results assume the best-fit dilution rate and the photolysis rates corresponding to the middle of the plume (solid black line in Fig. 4).

ACPD
14, 32427–32489, 2014

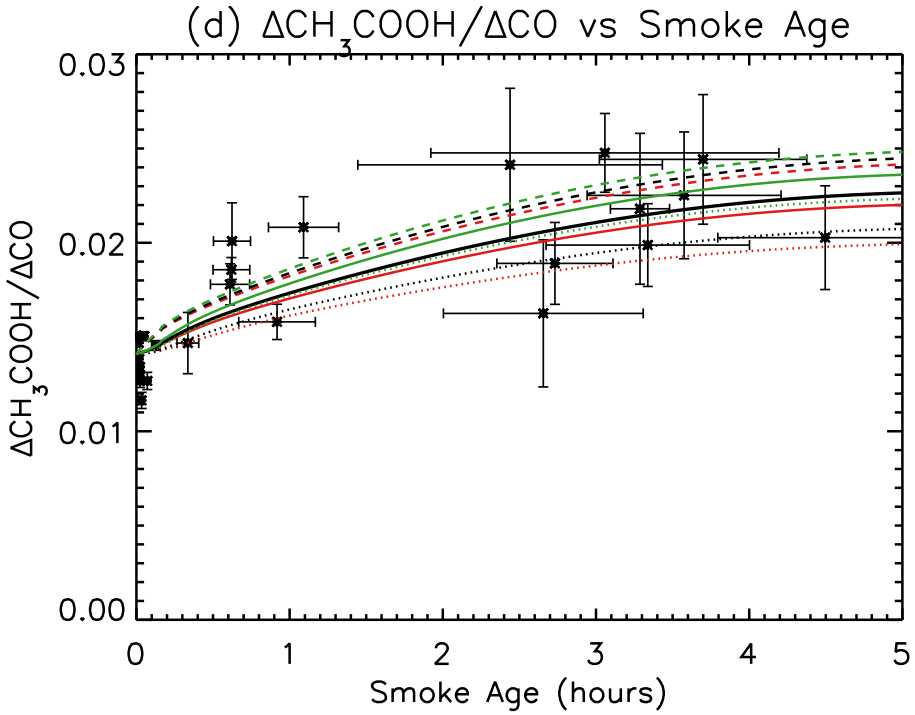

Figure 10. As in Fig. 8d, but for the "Half Fragmentation" SVOC mechanism (see Table 1) where the VOC fragment produced by fragmentation of the parent SVOC is assumed to become acetic acid.

ACPD
14, 32427–32489, 2014

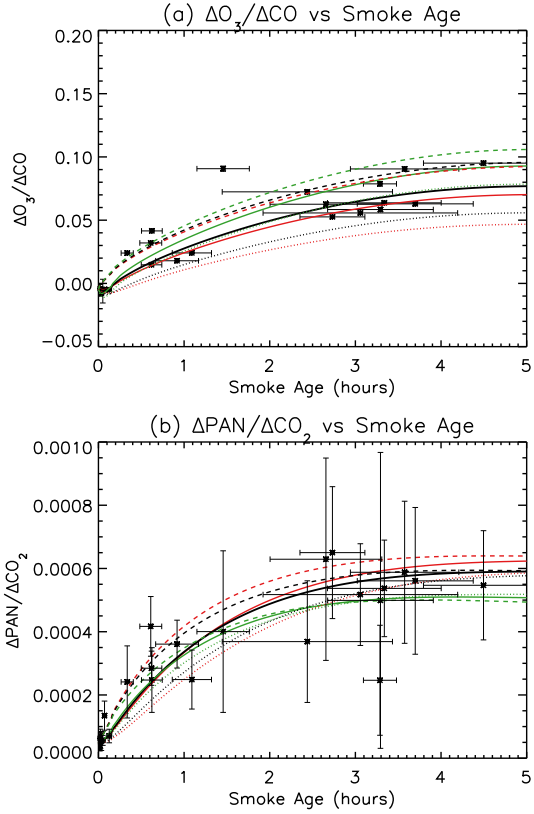

Figure 11. As in Fig. 5, but for the "Half Fragmentation" SVOC mechanism rather than no fragmentation (see Table 5).

ACPD
14, 32427–32489, 2014

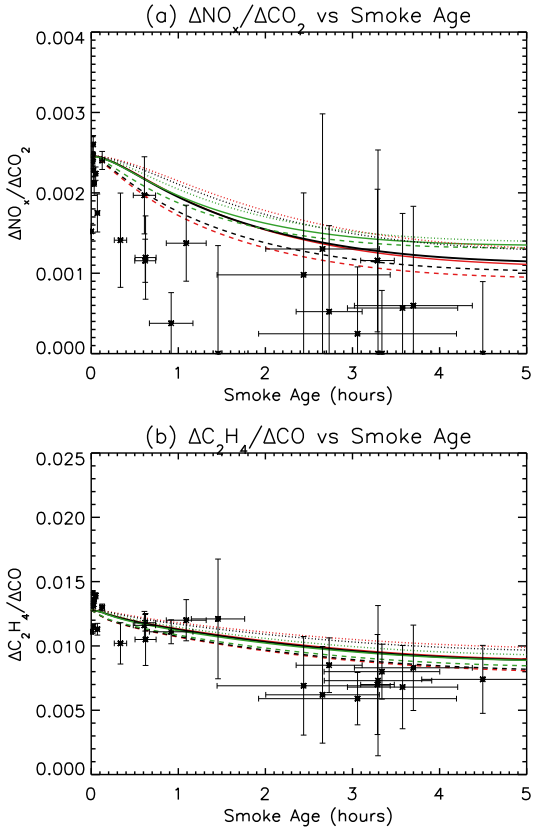

Figure 12. As in Fig. 6, but for the "Half Fragmentation" SVOC mechanism (see Table 5).

ACPD
14, 32427–32489, 2014

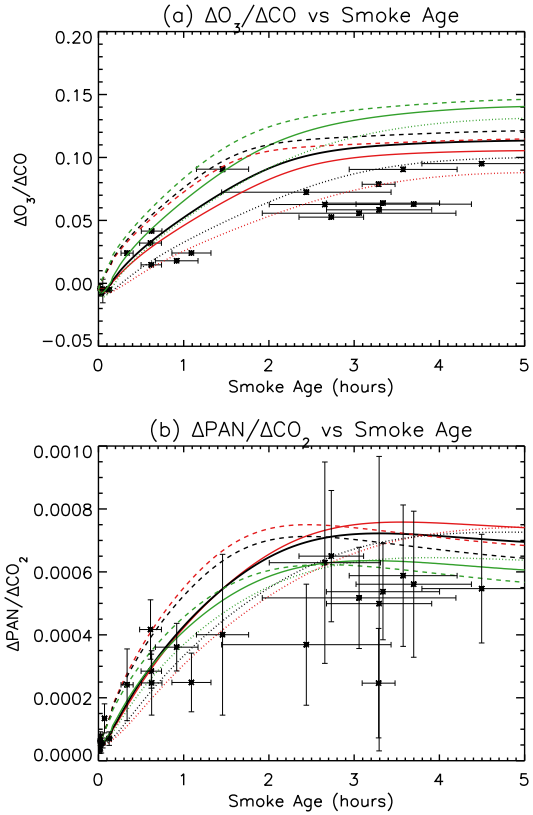

Figure 13. As in Fig. 5, but for the optimized SVOC chemistry (see Table 5).

ACPD
14, 32427–32489, 2014

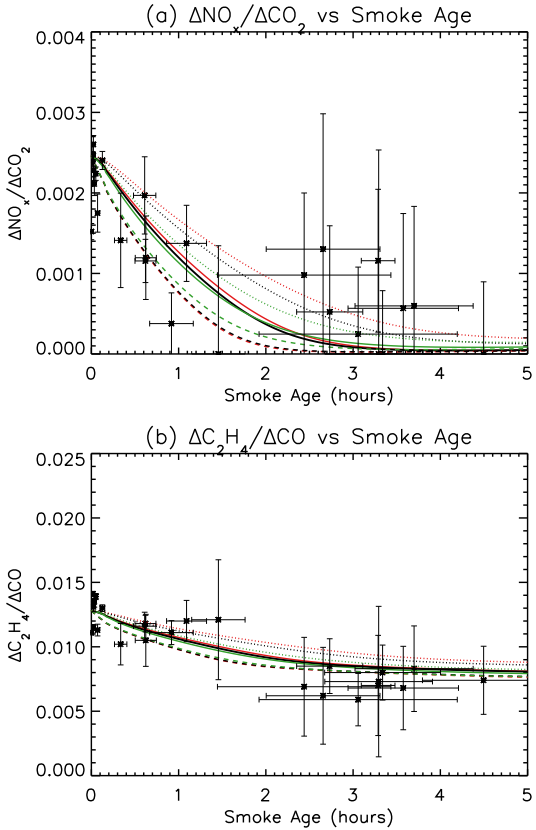

Figure 14. As in Fig. 6, but for the optimized SVOC Chemistry (see Table 1).

ACPD
14, 32427–32489, 2014